TECHNISCHE UNIVERSITÄT WIEN

MEDIZINISCHE UNIVERSITÄT WIEN

Master's Thesis

Hydraulic Characterisation of a Micro Vascular Plug for the Pulmonary Flow Reduction in Patients with Congenital Heart Disease

In partial fulfilment of the requirements for the degree of

Master of Science
in Biomedical Engineering

by

Niccolò Crescenti

under the supervision of

Ap. Prof. Marcus Granegger, PhD [1]
Assistant Prof. Dipl.-Ing. Bernhard Semlitsch, PhD [2]

[1] Department of Cardiac Surgery, Medical University of Vienna, Austria
[2] Research Unit of Fluid Flow Machinery, Vienna University of Technology, Austria

Die approbierte gedruckte Originalversion dieser Diplomarbeit ist an der TU Wien Bibliothek verfügbar
The approved original version of this thesis is available in print at TU Wien Bibliothek.
TU Bibliothek Your knowledge hub

Contents

Abbreviations **vii**

Abstract **ix**

1 Introduction **1**
1.1 Background . . . 1
1.1.1 The Heart . . . 1
1.1.2 Congenital Heart Diseases . . . 4
1.2 Surgical procedure . . . 8
1.2.1 The Nordwood procedure . . . 9
1.2.2 The Glenn procedure . . . 10
1.2.3 The Fontan procedure . . . 11
1.3 Advanced HLHS treatment approaches . . . 13
1.4 Micro Vascular Plugs (MVP) as Pulmonary Flow Restrictors (PFR) . . . 14
1.4.1 Clinical studies . . . 16
1.4.2 Major complications . . . 17
1.5 Aim of this project . . . 18

2 Materials & Methods **20**
2.1 In Vitro Experimental Analysis . . . 20
2.1.1 Mock loop set up . . . 20
2.1.2 Patient-specific geometry extraction . . . 24
2.2 In Silico Numerical Analysis . . . 26
2.2.1 Simulation set up . . . 28
2.3 Washout with the passive scalar approach . . . 31
2.4 Thrombus Formation Risk Model . . . 32
2.4.1 The Virchow's triad . . . 32
2.4.2 The Model . . . 33
2.5 Paraflow and flow through an orifice . . . 35

Die approbierte gedruckte Originalversion dieser Diplomarbeit ist an der TU Wien Bibliothek verfügbar
The approved original version of this thesis is available in print at TU Wien Bibliothek.
TU Bibliothek Your knowledge hub WIEN

3 Results **38**
3.1 In Vitro Experimental Results 38
3.1.1 Analytical Results 41
3.2 Numerical Results 46
3.3 Washout Outcome 52
3.4 Thrombus Risk Formation 52

4 Discussion **55**

5 Conclusion **62**

A Anatomical Planes & Directions **68**

B Maximum Pressure Gradient **69**

C Feedback Loop on Simulink **72**

D Thrombus Formation Risk Model on Star CCM+ **75**
D.1 Source terms 75
D.2 Mechanical and Chemical Activation 75
D.3 Scalar Shear Stress 76

E Error Measurements **77**

F Washout Results **78**
F.1 No hole 78
F.2 1 hole 80
F.3 2 holes 81

Die approbierte gedruckte Originalversion dieser Diplomarbeit ist an der TU Wien Bibliothek verfügbar
The approved original version of this thesis is available in print at TU Wien Bibliothek.
TU Bibliothek Your knowledge hub WIEN

List of Figures

1.1 Anatomy of a healthy heart 2
1.2 Wiggers diagram 3
1.3 Anatomy of a hypoplastic left ventricle heart 5
1.4 Sketched cardiovascular circulation before the Noordwood procedure 8
1.5 Sketched cardiovascular circulation with changes occurring during Nordwood procedure 9
1.6 Sketched cardiovascular circulation with changes occurring during Glenn procedure 11
1.7 Sketched cardiovascular circulation with changes occurring during Fontan procedure 12
1.8 Sketched cardiovascular circulation after the Fontan procedure 12
1.9 Parallel pulmonary and systemic resistances 13
1.10 Additional resistance R in the pulmonary circulation 14
1.11 Picture and sketch of the MVP in an unconstrained state . . . 15
1.12 Position after implant of the MVPs in the RPA and LPA . . . 15
1.13 MVP fenestration types 16

2.1 Top view of the MCL set-up 20
2.2 Sketch of the MCL set-up 21
2.3 Modified MVP featuring 2 holes 23
2.4 MVP placed in the 4.8 mm diameter pipe with the two struts on the left to avoid migration 23
2.5 Analytical models of Merrill (17), Einstein (12), Pries et al. (21), and experimental results of Rand et al. (22) for representing the relation of the haematocrit of human blood to viscosity 24
2.6 Patient geometry for in vitro tests 25
2.7 Set-up for 3D scan 26
2.8 Elliptical shape for MVP's perforation(s) 27

Die approbierte gedruckte Originalversion dieser Diplomarbeit ist an der TU Wien Bibliothek verfügbar
The approved original version of this thesis is available in print at TU Wien Bibliothek.
TU Bibliothek Your knowledge hub WIEN

2.9 Dimensions of the MVP and cylinder to define the fluid region with NX software . . . 28
2.10 Mesh independence analysis for MVP with No Hole at $Q = 0.1$ L/min . . . 29
2.11 Mesh outcome . . . 30
2.12 Virchow's Triad . . . 32
2.13 Sketches of MVP and analogy with flow through a circular orifice 36

3.1 Average pressure drop curves for four samples across unmodified MVP . . . 38
3.2 Average pressure drop curves for four samples across MVP with one and two holes . . . 39
3.3 Average pressure drop curves for four samples across different vessel diameters and compliance for flow rates ranging from 0 to 2 L/min (influence of perforation choice) . . . 40
3.4 Pressure-flow curve for the 3D-printed geometry . . . 42
3.5 Pressure-Flow curves in vitro vs. analytical formula . . . 42
3.7 Image series of MVP's diameter size reduction . . . 45
3.8 MVP radius as a function of the volume flow rate . . . 45
3.9 Pressure-Flow curves in vitro vs. in silico . . . 46
3.10 CFD - Flow Velocity Fields . . . 48
3.11 CFD - Stagnation Flow . . . 49
3.12 CFD - Wall Shear Stress . . . 50
3.13 CFD - Static Pressure . . . 51
3.14 Residuals of passive scalar for residence blood time . . . 52
3.15 Scaled volume average of the AP concentration for each of the three MVP configurations . . . 53
3.16 CFD - Thrombus model . . . 54

4.1 Sketched Pressure-Flow curve distribution for a MVP with one hole . . . 56
4.2 Drawings of the two flow distributions . . . 58
4.3 Pressure-flow curves comparison with results by Kizilski et al. 59

A.1 Human body, featuring anatomical planes and directions . . . 68

B.1 MVP Free body diagram and pressure distribution . . . 69

C.1 Simulink - Calibration of the flow sensor . . . 72
C.2 Simulink - Monitoring circuit . . . 73
C.3 Simulink - Feedback loop on the flow to control the gear pump 74

Die approbierte gedruckte Originalversion dieser Diplomarbeit ist an der TU Wien Bibliothek verfügbar
The approved original version of this thesis is available in print at TU Wien Bibliothek.
TU Bibliothek Your knowledge hub WIEN

F.1 Washout of unperforated MVP 79
F.2 Washout of MVP with one hole 80
F.3 Washout of MVP with two holes 81

Die approbierte gedruckte Originalversion dieser Diplomarbeit ist an der TU Wien Bibliothek verfügbar
The approved original version of this thesis is available in print at TU Wien Bibliothek.
TU Bibliothek Your knowledge hub WIEN

List of Tables

1.1 Geometrical parameters of the MVP in an unconstrained state 15

2.1 Pipes characteristics 22
2.2 MVP characteristics 23
2.3 Clear Resin V4 material properties 26
2.4 Side and frontal NX software rendering of the three MVP versions used in the numerical simulations 27
2.5 Mesh Quality Assessment table 29
2.6 Thrombosis risk model parameters 35

Die approbierte gedruckte Originalversion dieser Diplomarbeit ist an der TU Wien Bibliothek verfügbar
The approved original version of this thesis is available in print at TU Wien Bibliothek.

Abbreviations

ADP Adenosine Diphosphate

AP Active Platelets

ASD Arterial Septal Defect

CAD Computer-Aided Design

CFD Computational Fluid Dynamics

CHD Congenital Heart Diseases

CT Computed Tomography

DICOM Digital Imaging and Communication in Medicine

ECG Electrocardigram

HLHS Hypoplastic Left Heart Syndrome

IVC Inferior Vena Cava

LA Left Atrium

LPA Left Pulmonary Artery

LV Left Ventricle

MCL Mock Circulatory Loop

MVP Micro Vascular Plug

NP Non-active Platelets

PA Pulmonary Arteries

PAB Pulmonary Artery Banding

Die approbierte gedruckte Originalversion dieser Diplomarbeit ist an der TU Wien Bibliothek verfügbar
The approved original version of this thesis is available in print at TU Wien Bibliothek.
TU Bibliothek Your knowledge hub WIEN

PDA Patent Ductus Arteriosus

PFR Pulmonary Flow Restrictor

PTFE PolyTetraFluoroEthylene

PV Pulmonary Veins

Q_p Pulmonary flow rate

Q_s Systemic flow rate

RA Right Atrium

RMSE Root Mean Square Error

ROI Region of Interest

RPA Right Pulmonary Artery

RV Right Ventricle

SVC Superior Vena Cava

Die approbierte gedruckte Originalversion dieser Diplomarbeit ist an der TU Wien Bibliothek verfügbar
The approved original version of this thesis is available in print at TU Wien Bibliothek.
TU Bibliothek Your knowledge hub WIEN

Abstract

Purpose- Univentricular heart condition, such as the Hypoplastic Left Heart Syndrome (HLHS), denotes a severe Congenital Heart Disease (CHD). Newborn patients who are ineligible for a palliative surgical correction often suffer from pulmonary overperfusion and reduced systemic flow. This project aimed to hydraulically characterise a commercially available vascular plug (MVP - Medtronic, MN, USA) modified as a Pulmonary Flow Restrictor (PFR) and to investigate its personalisation towards a patient-specific approach to restore a balanced pulmonary-to-systemic (Q_p/Q_s) flow ratio.

Methods- First we focused on assessing the hydraulic resistance of Micro Vascular Plugs (MVPs) in a Mock Circulatory Loop (MCL). We measured the pressure drop across three different device configurations (no, one and two holes) for flow rates up to 2 L/min at steady-state conditions. Additionally, we tested varying pipe diameters and compliances. To have a more realistic environment, the measurements were also performed in a 3D-printed geometry obtained from a HLHS patient's Computed Tomography (CT) scan. Additional Computational Fluid Dynamics (CFD) simulations allowed to look further into hemodynamics, washout of passive scalar analysis and thrombus risk model implementation based on platelets' activation.

Results- The in vitro experiments revealed two key behaviours of the MVP in relation to flow rate. At low flow rates, hydraulic resistance is primarily determined by hole size, while at high flow rates, the pressure drop is mainly influenced by the ratio of MVP diameter to pipe diameter. The experimentally obtained results for hydraulic performance showed agreement with CFD simulations (RMSE = 2.5 mmHg for one hole and RMSE = 2.0 mmHg for two holes) and with analytical formulation (RMSE = 3.8 mmHg) at low flow rates (0 to 0.4 L/min). No major differences in washout time were observed between the one and two holes configurations of the MVP (approximately 0.48 s). Similarly, the thrombus risk model indicated minimal variation, with the scaled volume average of active platelet (AP) concentration increase differing by only 7% between the two configurations. The scaling

Die approbierte gedruckte Originalversion dieser Diplomarbeit ist an der TU Wien Bibliothek verfügbar
The approved original version of this thesis is available in print at TU Wien Bibliothek.
TU Bibliothek Your knowledge hub WIEN

was implemented such that the part per million (ppm) increase to the initial value of 25e12 m^{-3} was monitored.

Conclusion- Through in vitro and in silico investigations, we demonstrated that the hydraulic properties of the MVP can be personalized by adjusting the number of perforations and the MVP-to-pipe diameter ratio. Future studies will need to incorporate patient-specific parameters to tailor the MVP to individual needs towards improved patient outcomes.

Die approbierte gedruckte Originalversion dieser Diplomarbeit ist an der TU Wien Bibliothek verfügbar
The approved original version of this thesis is available in print at TU Wien Bibliothek.
TU Bibliothek Your knowledge hub WIEN

Die approbierte gedruckte Originalversion dieser Diplomarbeit ist an der TU Wien Bibliothek verfügbar
The approved original version of this thesis is available in print at TU Wien Bibliothek.

Chapter 1

Introduction

1.1 Background

1.1.1 The Heart

This research project focuses on the cardiovascular system, specifically addressing the congenital condition known as Hypoplastic Left Heart Syndrome (HLHS). To grasp the severity of the HLHS, it is essential to first understand the heart's anatomy, its functions, and its critical role in maintaining hemodynamic homeostasis, the regulation of blood circulation, to ensure that tissues receive an adequate supply of oxygen and nutrients.

Anatomy

The heart is a four-chamber organ (see Figure 1.1), with two upper chambers, the atria, and two lower chambers, the ventricles. The right, respectively, left atrium and ventricle are commonly referred to as the right, respectively, left heart. The Left Atrium (LA) receives blood from the Pulmonary Veins (PV), it flows into the Left Ventricle (LV) through the mitral valve, and then is sent to the aorta. The Right Atrium (RA) receives blood from both the Inferior Vena Cava (IVC) and Superior Vena Cava (SVC), flows into the Right Ventricle (RV) through the tricuspid valve and is then sent into the main Pulmonary Arteries (PA).

For the heart to work as a pump, it needs contractile muscular tissue to generate mechanical contraction. There are three main muscle categories in the human body [1]:

- *Skeletal muscles* responsible for voluntary movements such as walking;

- *Smooth muscles* responsible for involuntary movement like moving food through the digestive tract or controlling the diameter of blood vessels;
- *Cardiac muscles* responsible for involuntary pumping of the blood.

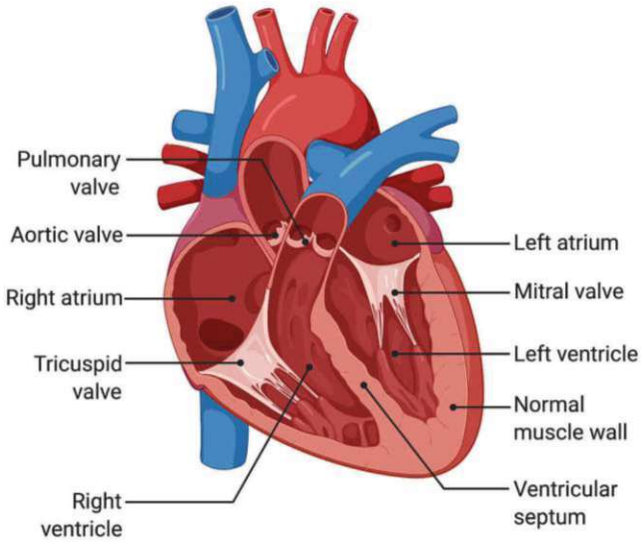

Figure 1.1: *Anatomy of a healthy heart. Oxygenated blood is in red and deoxygenated is blood in blue* [2].

There are two different types of cardiac muscle cells. Unlike skeletal muscle cells - necessitating external stimulation for contraction - some cardiac muscle cells can spontaneously produce action potentials,[1] they belong to the so-called pacemaker cells [3]. The other ones, much more abundant - making up 99% of the cardiac muscle cells [4] - are the non-pacemaker cells, also called myocardial contractile cells as they are primarily responsible for the heart's contractions.[2]

The heart pumps blood with a rhythm that is imposed by the pacemaker cells in the sinoatrial node, and the signal is spread throughout the heart by the conduction system/electrical pathway. The ability of pacemaker cells to generate a spontaneous cardiac action potential and, therefore, the contraction of the heart without any outside signal is a unique property of the heart called *autorhythmicity* [1].

[1]The action potential will lead to the contraction of electrically interconnected cardiac muscle cells.

[2]The pacemaker cells are less contractile elements.

Die approbierte gedruckte Originalversion dieser Diplomarbeit ist an der TU Wien Bibliothek verfügbar
The approved original version of this thesis is available in print at TU Wien Bibliothek.

The cardiac cycle and the Wiggers diagram

The collection of events that occur during each heartbeat, both mechanical and electrical processes, forms the so-called cardiac cycle. It is divided into two main phases for the atria and ventricles: *diastole* (relaxation) and *systole*[3] (contraction). Let's consider the cardiac cycle of the left heart. The sequence can be resumed in what is called a Wiggers diagram after its developer (see Figure 1.2).

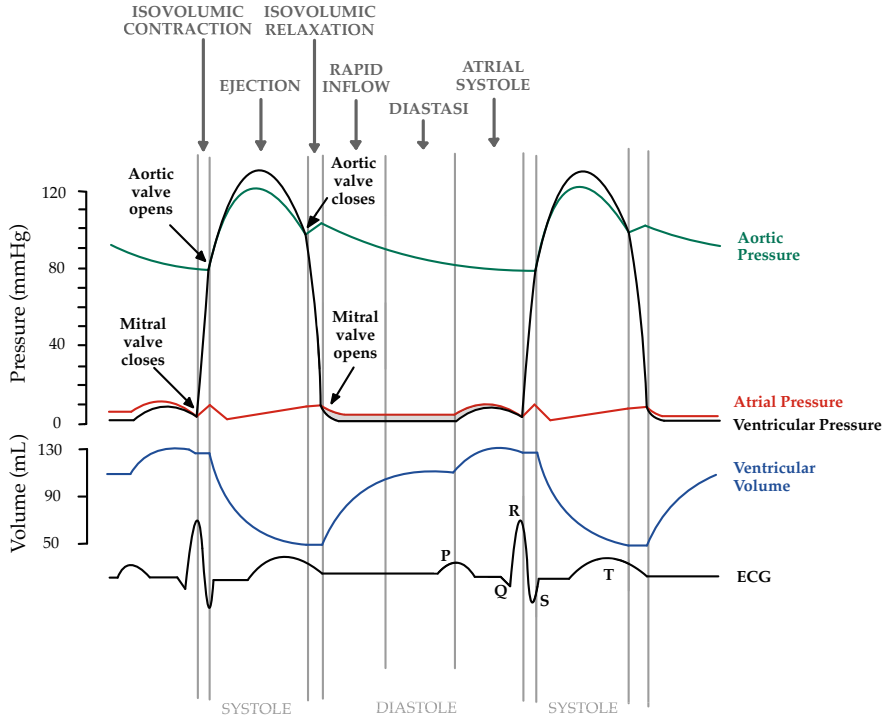

Figure 1.2: *The Wiggers diagram featuring the different pressures, the left ventricular volume and the Electrocardigram (ECG) corresponding to the left ventricle during two cycles* [5].

The cardiac cycle begins with *atrial contraction*. The increase of atrial pressure forces the blood into the ventricle as the ventricular pressure is lower. The ventricle fills with blood. Once the ventricle is filled with blood and the contraction starts, the ventricular pressure is higher than in the atria, and the mitral valve closes. For a moment, the aortic valve remains closed as well and the ventricle contracts at constant volume, it's the *isovolumetric contraction*. Ventricular ejection is triggered when the ventricular pressure

[3]If not mentioned, the systole and diastole refer to the ventricles.

Die approbierte gedruckte Originalversion dieser Diplomarbeit ist an der TU Wien Bibliothek verfügbar
The approved original version of this thesis is available in print at TU Wien Bibliothek.

exceeds the pressure within the aorta. The *ejection* phase terminates when the ventricular pressure drops below the aortic pressure. It is the end of systole and the beginning of diastole. The ventricle relaxes with all valves closed, it is the *isovolumetric relaxation*. Ventricular pressure keeps dropping at constant volume. Meanwhile, the atrium is filling with blood, building up pressure. As the atrial pressure exceeds the ventricular pressure, the blood starts flowing from the atrium to the ventricle. The last amount of blood is pushed actively by *atrial contraction* and the cycle starts again.

During ventricular diastole, aortic blood pressure reaches roughly 80 mmHg, whereas during ventricular systole, aortic blood pressure reaches higher values, roughly 120 mmHg.[4]

The circulatory system

Blood circulation is crucial for the transport of oxygen and nutrients to all the organs, and to ensure heat exchanges [7]. In the human body, blood is pumped into two different circulations. One is a short, low-pressure circuit: the *pulmonary circulation*. From the RV, blood enters the pulmonary artery directed to the lungs then back to the heart through the PV and enters the LA. In the pulmonary circulation, blood gets oxygenated. The other one is a long, high-pressure circuit: the *systemic circulation*. From the LV, blood flows into the aorta directed to the organs and muscles of the body then back to the heart through the IVC and SVC and enters the RA. Due to the uptake of oxygen from the organs, blood gets deoxygenated in the systemic circulation. Proper blood flow circulation is therefore essential for a human to thrive. Not only does it provide rapid transport of oxygen, nutrients, hormones and other metabolic substances crucial for survival, but it also fulfils other tasks such as heat transportation, blood redistribution - according to organ demands - and generates pressure forces for filtration (e.g. kidneys).

1.1.2 Congenital Heart Diseases

The leading cause of death worldwide is linked to diseases related to a dysfunction of the cardiovascular system [8]. They can be separated into two categories, according to the origin. Some of them are congenital, hence present from birth, all the others are acquired, hence encountered after birth. Among all the abnormal cardio-circulatory structures, this project focuses on HLHS.

[4]These two values are optimal maximum blood pressure values as far as cardiovascular risks are concerned [6].

Die approbierte gedruckte Originalversion dieser Diplomarbeit ist an der TU Wien Bibliothek verfügbar
The approved original version of this thesis is available in print at TU Wien Bibliothek.
TU Bibliothek Your knowledge hub WIEN

Hypoplastic Left Heart Syndrome

HLHS accounts for up to 3.8% of Congenital Heart Diseases (CHD). Despite the relatively low incidence, it is responsible for 23% of cardiac deaths occurring in the first week of life [9]. It is a condition characterised by single-ventricle physiology (see Figure 1.3) or other underdevelopment of left side structure[5] in which one ventricle, in this case the RV, is responsible for pumping blood to both systemic and pulmonary circulations. With these two circulations operating in parallel, blood follows the path of least resistance. If the resistances of the two circulations were equal, blood flow would distribute evenly between them. However, in HLHS, the resistance in the systemic circulation is significantly higher than in the pulmonary circulation. This can often result in pulmonary overperfusion, hence high pressure in the pulmonary circuit, putting the patient at risk. While immediate surgery is required, many neonates are too fragile to be immediately operated on, necessitating a bridging strategy to control flow ratios first and stabilise the patient until surgery is feasible.

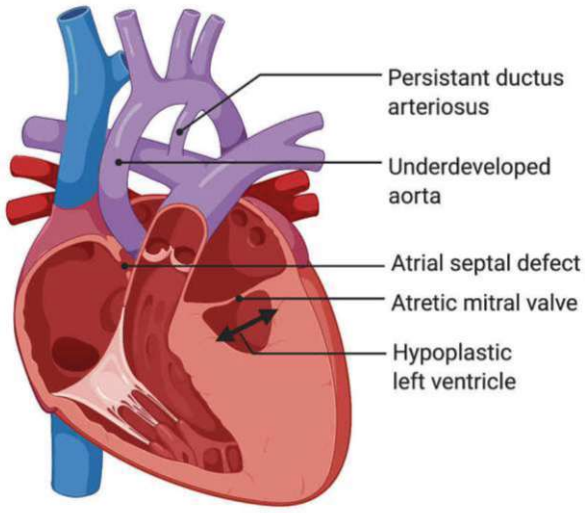

Figure 1.3: *Anatomy of a hypoplastic left ventricle heart. Oxygenated blood is depicted in red and deoxygenated blood in blue. Both the left ventricle and the aorta are much smaller compared to those in a healthy heart. Only a small amount of blood is pumped into the systemic circulation. Moreover, it is not only oxygenated blood but a mixture, as purple stands for mixed blood* [2].

[5]HLHS also encloses other malformations of the left side of the heart concerning the mitral valve and the aorta [10].

Die approbierte gedruckte Originalversion dieser Diplomarbeit ist an der TU Wien Bibliothek verfügbar
The approved original version of this thesis is available in print at TU Wien Bibliothek.

Pulmonary overcirculation and the Q_p/Q_s ratio

One of the critical challenges of HLHS is linked with pulmonary overperfusion. Such a condition is observed when too much blood flows into the pulmonary circulation compared to the blood that flows into the systemic circulation. Mathematically, it simply translates as:

$$Q_p > Q_s, \tag{1.1}$$

where Q_p and Q_s are respectively the pulmonary and systemic blood flow.

As we presented shortly in section 1.1.2, HLHS refers to a wide spectrum of left heart anatomical structure defects. The presence of which inevitably leads to a distortion within the systemic circulation [11]. In some extreme cases, even to a partial or total occlusion of vessels. Considering that both the circulatory and metabolic homeostasis in patients with HLHS is dependent on a delicate balance between systemic and pulmonary blood flow, getting the right Q_p/Q_s ratio and keeping it under control, hence allowing only small deviations from target value, is of great deal [12].

After birth, in balanced conditions, the pulmonary output is almost identical to the systemic output, hence:

$$\frac{Q_p}{Q_s} = 1.$$

In the case of HLHS, the ratio can reach higher values, such as 5:1 reported in [13], which requires special attention.

The way cardiologists and surgeons measure the Q_p/Q_s ratio is using Fick's law. To get to the equation of Q_p/Q_s, some variables need to be introduced first:

- V_{p,O_2}: pulmonary oxygen consumption [mL/min];
- V_{s,O_2}: systemic oxygen consumption [mL/min];
- C_{a,O_2}: arterial blood oxygen content [mL O_2/dL];
- C_{pv,O_2}: pulmonary venous blood oxygen content [mL O_2/dL];
- C_{mv,O_2}: mixed venous blood oxygen content [mL O_2/dL].

Die approbierte gedruckte Originalversion dieser Diplomarbeit ist an der TU Wien Bibliothek verfügbar
The approved original version of this thesis is available in print at TU Wien Bibliothek.

Fick's principle states that:

"The total uptake of (or release of) a substance by the peripheral tissues is equal to the product of the blood flow to the peripheral tissues and the arterial-venous concentration difference (gradient) of the substance." [14]

If we consider oxygen uptake taking place in the pulmonary circulation, the principle translates into the following equation:

$$V_{p,O_2} = Q_p(C_{pv,O_2} - C_{a,O_2}),$$

or in terms of the flow rate:

$$Q_p = \frac{V_{p,O_2}}{C_{pv,O_2} - C_{a,O_2}}.$$

Similarly, for the systemic blood flow, we get:

$$Q_s = \frac{V_{s,O_2}}{C_{mv,O_2} - C_{a,O_2}}$$

Then the Q_p/Q_s ratio simply becomes:

$$\frac{Q_p}{Q_s} = \frac{C_{a,O_2} - C_{mv,O_2}}{C_{pv,O_2} - C_{a,O_2}}$$

Usually, the oxygen content is difficult to measure. It is much easier to measure oxygen saturation [15] and use the following equation to retrieve the oxygen content:

$$\begin{aligned}\text{Oxygen Content [mL } O_2\text{/dL]} = \text{Haemoglobin [g/dL]}\times \\ 1.34 \text{ [mL } O_2\text{/g]} \times \text{Oxygen Saturation [\%]}+ \\ 0.003 \text{ [mL } O_2\text{/dL/mmHg]} \times \text{Pa}O_2 \text{ [mmHg]}\end{aligned}$$

with PaO_2 the partial pressure of oxygen. From the equation, we see that oxygen content appears in two forms: oxygen bound to haemoglobin and dissolved oxygen. Since the second term is much smaller than the first one, we can make the approximation:

$$\begin{aligned}\text{Oxygen Content [mL } O_2\text{/dL]} = \text{Haemoglobin [g/dL]}\times \\ 1.34 \text{ [mL } O_2\text{/g]} \times \text{Oxygen Saturation [\%]}.\end{aligned}$$

Die approbierte gedruckte Originalversion dieser Diplomarbeit ist an der TU Wien Bibliothek verfügbar
The approved original version of this thesis is available in print at TU Wien Bibliothek.
TU Bibliothek Your knowledge hub WIEN

Therefore, after simplification, we get the expression of the Q_p/Q_s ratio in terms of oxygen saturation as :

$$\frac{Q_p}{Q_s} = \frac{S_{a,O_2} - S_{mv,O_2}}{S_{pv,O_2} - S_{a,O_2}}. \tag{1.2}$$

By measuring the oxygen saturation in the blood vessels, clinicians can measure the Q_p/Q_s ratio. After cardiac catheterizations, the saturations are measured in the aorta, PV, IVC and SVC [16].

1.2 Surgical procedure

Newborns with HLHS face two main treatment options: heart transplant or the creation of the so-called "Fontan circulation" [17]. Considering that the availability of donor organs is limited, especially for children, the second option, a palliative one,[6] is carried out more frequently and reports long-term survival rates (25–30 years) ranging from less than 43 to 76% [18]. It is obtained by carrying out three main operations in the following order: the Nordwood, the Glenn, and the Fontan procedure.

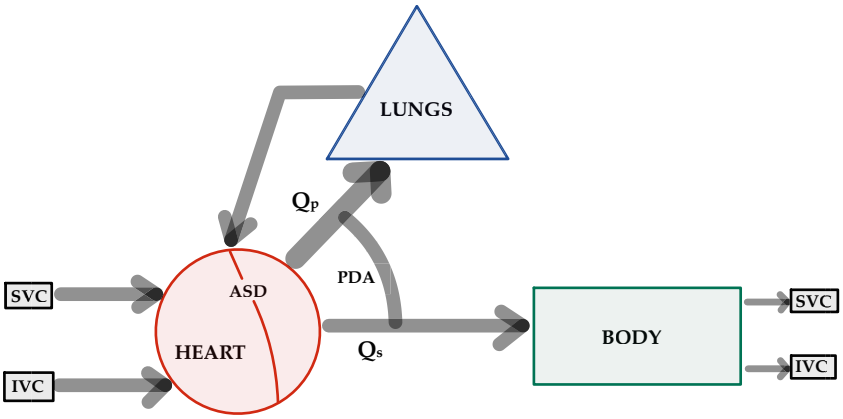

Figure 1.4: *Sketched cardiovascular circulation before the Noordwood procedure. High Q_p/Q_s ratio, presence of the Patent Ductus Arteriosus (PDA) and small Arterial Septal Defect (ASD).*

[6] i.e. relieve of the symptoms without dealing with the cause of the condition.

Die approbierte gedruckte Originalversion dieser Diplomarbeit ist an der TU Wien Bibliothek verfügbar
The approved original version of this thesis is available in print at TU Wien Bibliothek.

1.2.1 The Nordwood procedure

The Norwood procedure is the first stage palliative procedure performed within the first weeks of life. It aims to make it possible for the right ventricle to pump blood to the whole body (systemic circulation) as well as to the lungs (pulmonary circulation) as it usually does. It provides unobstructed systemic blood flow and adequate coronary perfusion to sustain the heart. Four main modifications appear during the Norwood procedure [19]:

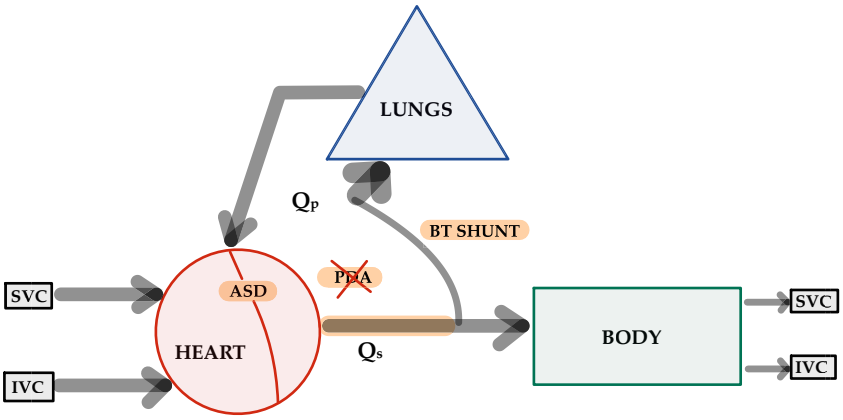

Figure 1.5: *Sketched cardiovascular circulation with changes occurring during Nordwood procedure. The changes involve: the building of a "new" aorta, the addition of a shunt between the aorta and pulmonary arteries, the closure of the PDA and the enlargement of the ASD.*

- Build of a "new" aorta; the proximal part, close to the heart, of the pulmonary artery is connected to the aorta. A bigger aorta now goes from the right ventricle to the body, overcoming the problem of low perfusion due to a very narrow aorta.
- Add of a shunt path, to keep blood flowing into the pulmonary circulation since the pulmonary artery brings new blood into the systemic circulation.
- Closure of the PDA; the PDA is a small aperture between the two main blood vessels leaving the heart: the aorta and the pulmonary artery. It lets oxygen-rich blood mix with oxygen-poor blood. It is found in babies before and just after birth. In a healthy heart, it will shrink and close on its own in the first few days of life. For HLHS-affected babies, it will stay open longer which causes extra blood into the pulmonary

Die approbierte gedruckte Originalversion dieser Diplomarbeit ist an der TU Wien Bibliothek verfügbar
The approved original version of this thesis is available in print at TU Wien Bibliothek.

circulation, thus to the lungs. Up to now, the PDA needed to be open, so blood could flow from the right ventricle into the systemic circulation. However, this task is now fulfilled by the "new", larger aorta. The PDA is therefore not needed any more.

- Enlargement of the Atrial Septal Defect (ASD); the ASD is a birth defect that manifests itself through a small hole in the septum (wall) that divides the two atria. This hole can vary in size. A small one will close by itself. However, larger ones might require surgery to reduce any risk of further complications. A hole between the two upper chambers of the heart will enable blood-rich and poor oxygen to mix. In the case of HLHS, it is a positive feature. As the right ventricle now pumps blood into the systemic circulation, therefore to the body tissues that require oxygenated blood, an enlarged ASD lets more oxygenated blood enter the right ventricle.

After the Nordwood procedure, thanks to the enlargement of the aorta, the additional shunt, the removal of the PDA and the enlargement of the ASD, blood is pumped into the parallel pulmonary and systemic circulations entirely by the right ventricle. Due to all these different changes, the Norwood procedure is one of the most delicate ones to achieve. After that, babies usually need 3 to 4 weeks of recovery [19]. 3 to 6 months later, the next surgery will be needed.

1.2.2 The Glenn procedure

The Glenn procedure is performed after 3 to 6 months of life. As the Norwood procedure, it is an open-heart surgery type. So far, since the left ventricle is too small, the right ventricle is pumping the blood in both the pulmonary and the systemic circulations (in parallel), therefore not only to the lungs but also to the body tissues. As the circulations are in parallel, it requires the heart to work much harder in terms of volume than it would in a healthy patient. The Glenn procedure aims to alleviate the heart's work by sending the blood from the upper body directly towards the lungs, as the upper body and pulmonary circulation are in series and parallel to the lower body. Indeed, connecting the SVC to the PA allows poor-oxygenated blood to flow straight to the lungs [20].

- The SVC is disconnected from the heart and connected directly to the pulmonary artery. In this way, the poor-oxygenated blood from the upper body goes directly to the lungs without the need to flow through the heart.

Die approbierte gedruckte Originalversion dieser Diplomarbeit ist an der TU Wien Bibliothek verfügbar
The approved original version of this thesis is available in print at TU Wien Bibliothek.
TU Bibliothek Your knowledge hub WIEN

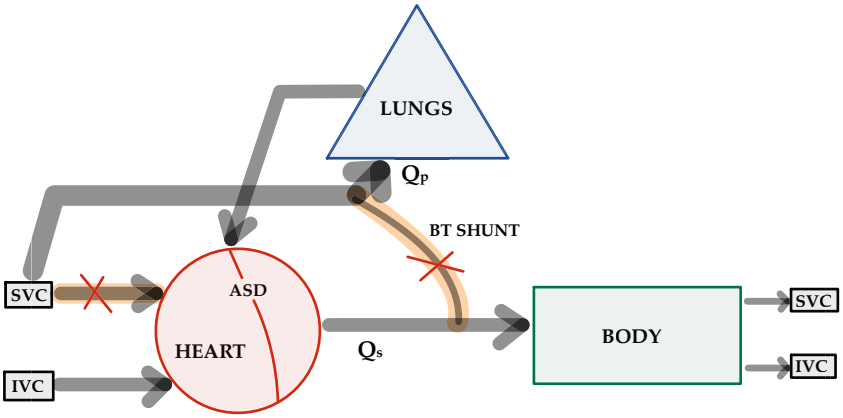

Figure 1.6: *Sketched cardiovascular circulation with changes occurring during Glenn procedure. The changes include the disconnection of the SVC from the heart and the removal of the shunt previously added.*

- Removal of the shunt from the Norwood procedure. Since the additional shunt was there to make sure that the right ventricle was also pumping part of the blood to the lungs, it was not needed any more.

To resume, the Glenn procedure improves blood circulation. The poor-oxygenated blood from the upper body doesn't flow through the heart, where the circulation is impaired, and the work is already hard. Instead, it is directed to the lungs. After the Glenn procedure, the patient will need to recover for 1 to 2 weeks [20]. A next surgery will then be needed.

1.2.3 The Fontan procedure

The Fontan procedure is usually performed after 18 to 36 months of life. After the Glenn procedure, the issue that persists is that all the deoxygenated blood from the lower body still keeps flowing into the systemic circulation, meaning that blood with poor oxygen content is still mixing with blood with high oxygen content. Body tissues might not receive the required amount of oxygen they need to function properly. The aim of the Fontan procedure is to ensure that the heart doesn't only pump blood into the systemic circulation, to the body, but that the blood that is pumped into the body is rich in oxygen. Both circulations are in series. Two main changes occur during the Fontan procedure [21]:

- IVC is disconnected from the heart. The poor-oxygenated blood from the lower body is now flowing directly to the lungs. Usually, a conduit is added for the IVC and the PA to be connected.

Die approbierte gedruckte Originalversion dieser Diplomarbeit ist an der TU Wien Bibliothek verfügbar
The approved original version of this thesis is available in print at TU Wien Bibliothek.

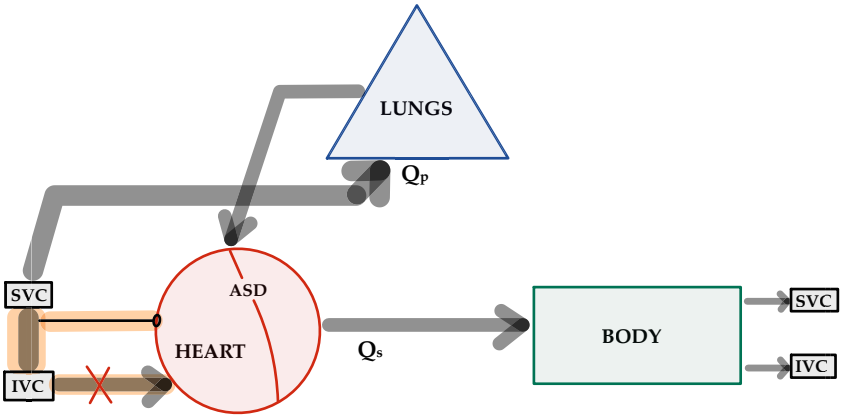

Figure 1.7: *Sketched cardiovascular circulation with changes occurring during Fontan procedure. The major change involves the disconnection of the IVC from the heart.*

- Creation of a small hole in the right atrium. Between the newly added conduit and the right atrium, a small fenestration is made to let part of the blood from the lower body flow back into the heart. This is done to avoid too much blood, therefore too much pressure, flowing right away to the lungs.

Thanks to the Fontan procedure, there is no more mixture of poor-oxygenated blood with rich-oxygenated blood that enters the systemic circulation. Blood from the lower body now goes directly to the lungs and the right ventricle acts as the main and only pump responsible for the blood flow in the whole body.

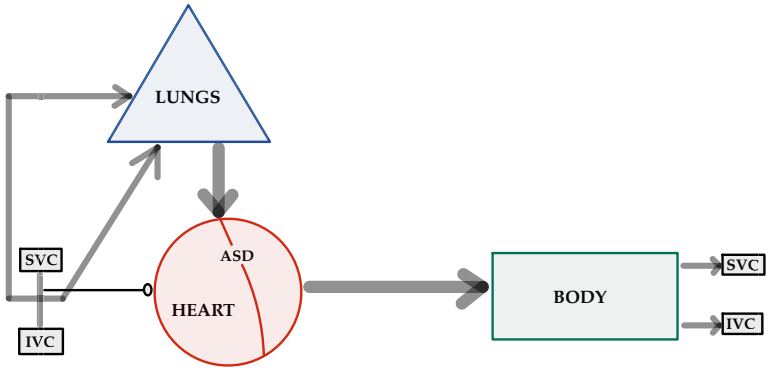

Figure 1.8: *Sketched cardiovascular circulation after the Fontan procedure. Blood flows in a single loop.*

Die approbierte gedruckte Originalversion dieser Diplomarbeit ist an der TU Wien Bibliothek verfügbar
The approved original version of this thesis is available in print at TU Wien Bibliothek.

1.3 Advanced HLHS treatment approaches

Bridge to candidacy

Every newborn in need should receive a palliative operation as soon as possible. However, not every patient is eligible at birth. It sometimes happens that some high-risk neonates do not have a health situation that is good enough to ensure their survival after the surgery. The causes for a fragile situation can be due to prematurity, low birth weight, major comorbidities, ventricular dysfunction and severe atrioventricular valve regurgitation [22]. For all these patients, a bridging therapy is needed that addresses the issue of pulmonary overcirculation, getting the Q_p/Q_s ratio under control to stabilize their condition first.

The discrepancy between the values of Q_p and Q_s is a reflection of the discrepancy between the pulmonary resistance R_p and the systemic resistance R_s. Since these resistances are in parallel, the analogy with electrical components makes it easier to understand that if one of the resistances is much higher, the related flow will be much smaller. In our case, it is the systemic resistance to be much higher than the pulmonary resistance.

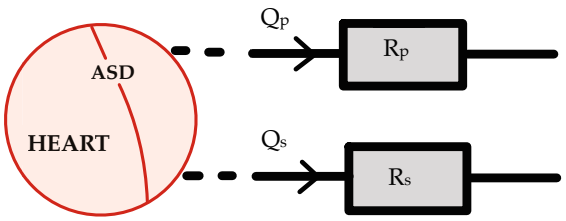

Figure 1.9: *Sketch of the pulmonary and systemic resistances in parallel.*

Indeed, if so, the equivalent resistance in Figure 1.9 is the pulmonary resistance:

$$R_{eq} = \frac{1}{\frac{1}{R_p} + \frac{1}{R_s}} = \frac{R_s R_p}{R_s + R_p} \simeq R_p \tag{1.3}$$

It is as if the flow in the systemic circulation is significantly reduced and blood flow is mostly directed towards the pulmonary circulation, as the only resistance considered is the pulmonary one.

Die approbierte gedruckte Originalversion dieser Diplomarbeit ist an der TU Wien Bibliothek verfügbar
The approved original version of this thesis is available in print at TU Wien Bibliothek.

Pulmonary Artery Banding

To get the Q_p/Q_s ratio under control in patients with single ventricle physiology, several techniques have been explored to increase the resistance in the pulmonary circulation, as is shown in Figure 1.10.

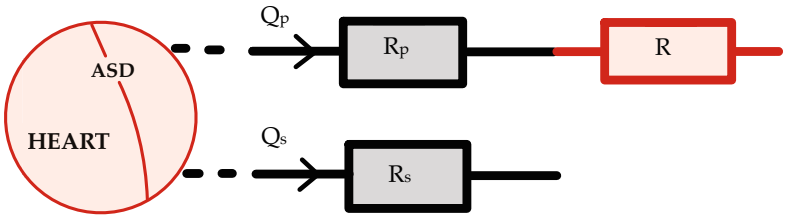

Figure 1.10: *Sketch of the additional resistance R (in red) needed to increase the overall resistance in the pulmonary circulation.*

Previously, it was achieved mainly by Pulmonary Artery Banding (PAB) [23], a technique which consists of the placement of a band by the surgeons around both pulmonary arteries and tightening it to reduce the lumen of the blood vessels and, consequently, reduce the blood flow rate. The main issue with this approach is that it involves open-heart surgery, which these fragile patients are unlikely to endure. It was therefore not the optimal bridging technique, and an alternative interventional method was needed. Researchers have continued to explore other options. Recently, the attention has been directed towards modified Micro Vascular Plug (MVP)s [24].

1.4 Micro Vascular Plugs (MVP) as Pulmonary Flow Restrictors (PFR)

A MVP is a self-expanding vessel occlusion medical device produced by Medtronic (Medtronic, Inc. Minneapolis, MN). It has an ovoid shape with a skeleton of nitinol wires and a PolyTetraFluoroEthylene (PTFE) membrane that covers roughly 75% of the device, left uncovered at the distal end[7] (see Figure 1.11a). It comes in different sizes, idealized for different vessel dimensions. The MVP-Q7 model was the one investigated in our research. Its geometrical dimensions are reported in Table 1.1. For the definition of the variables, please refer to Figure 1.11b.

[7]For anatomical planes and directions nomenclature, refer to Appendix A.

Die approbierte gedruckte Originalversion dieser Diplomarbeit ist an der TU Wien Bibliothek verfügbar
The approved original version of this thesis is available in print at TU Wien Bibliothek.

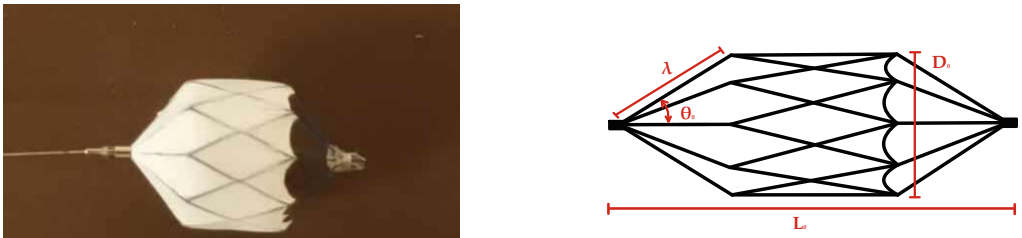

(a) MVP-Q7 (b) Parameters notation

Figure 1.11: *Picture (a) and sketch (b) of the MVP in an unconstrained state.*

L_0	D_0	λ	$\theta_0 = \sin^{-1}(D_0/2\lambda)$
16 mm	9.2 mm	5.7 mm	54°

Table 1.1: *Geometrical parameters of the MVP in an unconstrained state.*

This device is originally meant for peripheral embolisation. It is indicated by the manufacturer to be used to *obstruct* or *reduce* the rate of blood flow in the peripheral vasculature.[8] However, researchers have investigated the potential of such a device acting as a Pulmonary Flow Restrictor (PFR) once placed in the right and left PAs as shown in Figure 1.12.

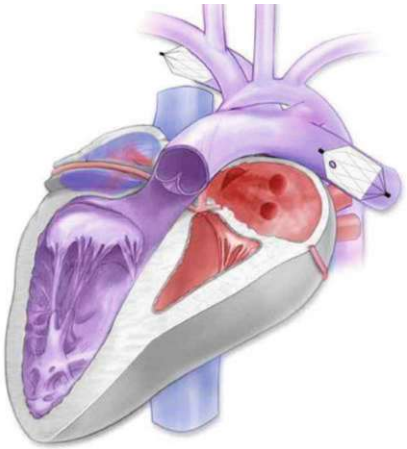

Figure 1.12: *Position after implant of the MVPs in the right and left PAs* [22].

[8]MVP™ micro vascular plug system - medtronic.com

Die approbierte gedruckte Originalversion dieser Diplomarbeit ist an der TU Wien Bibliothek verfügbar
The approved original version of this thesis is available in print at TU Wien Bibliothek.

1.4.1 Clinical studies

Establishing a controlled balance between Q_p and Q_s is critical for young patients to thrive. This necessity has driven the development of new approaches, such as using modified MVP as PFR, which has prompted numerous clinical studies [24] [25]. The goal is to restrict blood flow without completely blocking it, which requires modification of the device. This modification involves creating a fenestration, a small opening in the PTFE membrane. This aperture allows only a limited amount of blood to reach the lungs and enables the MVP to act as the hydraulic resistance depicted in red in Figure 1.10.

Several fenestration types are applied (see Figure 1.13): triangular, cross-shaped, circular [26] [22], diamonds [27]. The range of fenestration techniques is numerous as well: with a beaver mini-blade, Eye Bovie cautery (for circular hole) [28] [26] and surgical scalpel blade [27].

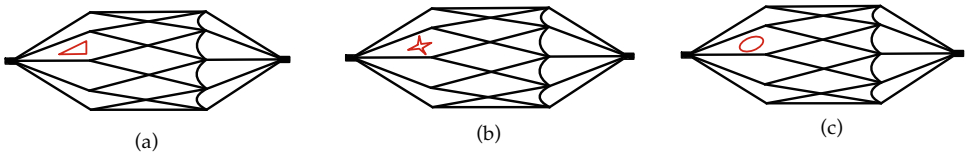

Figure 1.13: *Sketch of some of the fenestration types (in red) applied on the PTFE membrane of the MVP: triangular (a), cross-shaped (b) and circular (c).*

Once clinicians began exploring the use of modified MVPs as PFRs, the implantation procedure became standardized. This procedure typically involves single-stage ductal stenting, followed by the placement of bilateral modified MVPs via femoral access [28]. The major advantage over PAB is the avoidance of surgery.

The appeal of this approach also lies in the ease of uneventful explantation, as noted by Haddad et al. [25]. Most cases report a minimally invasive operation. The ease of implantation and explantation was investigated by Khan et al. [24] in a swine model as well. The study reported a 100% successful retrieval of the MVP after 3, 6 and 9 weeks post-implant and 50% at 12 weeks.

Following the animal experiments led by Khan et al. [24], the MVP were also implanted in humans. Schranz et al. [29] reported promising outcome

Die approbierte gedruckte Originalversion dieser Diplomarbeit ist an der TU Wien Bibliothek verfügbar
The approved original version of this thesis is available in print at TU Wien Bibliothek.
TU Bibliothek Your knowledge hub WIEN

in terms of feasibility. Similar to Nagotte et al. [28], only two out of six neonates needed additional operations. One needed removal and replacement of the MVPs, the second one needed left PA stenting.

Among the several advantages of using the MVP as PFR, the most important is its commercial availability [24]. It is already a device that is medically approved. Nonetheless, regardless of how promising this technique looks to be, some clinicians are cautious about its outspreading in clinical trials due to several factors such as the difficulty of modifying the device in an easy way and its migration risk.[24] [28].

1.4.2 Major complications

Modifiable Mechanism

As it currently stands, the MVP acts as a plug, significantly reducing or completely blocking fluid flow. To change it into a PFR, a small orifice must be created in the PTFE membrane. However, creating this perforation on the MVP is a challenging task, and not all techniques are easily executed. Among the methods discussed earlier, using a scalpel to create the hole is far more complex than using an eye Bovie, as experienced by Nageotte et al. [28]. A greater challenge lies in determining the optimal size of the fenestration, as an oversized perforation would cancel the benefits of using the MVP as a PFR, while an undersized perforation would result in excessively high pressure drop.

As Nagotte et al. points out, one additional important aspect is that once in place, there should be no flow around the device [28] as it would be an incentive for device migration. Throughout this work, we will refer to this flow as the paraflow. The ideal device would exert sufficient radial strength to resist the pressure exerted on it, preventing collapse under the force of the surrounding pressure field. This structural integrity is essential to avoid migration and as a consequence ensure consistent functionality as a flow restrictor.

Migration Risk

The interest of clinicians in the new approach of using MVPs as PFRs, and the rising of some concerns, led to a first in vitro investigation to understand the physiological consequences of such device implantation. In addition to a case series report over 8 patients, Kizliski et al. conducted in vitro analysis in a Mock Circulatory Loop (MCL) and developed an analytical model for device migration risk [26].

Die approbierte gedruckte Originalversion dieser Diplomarbeit ist an der TU Wien Bibliothek verfügbar
The approved original version of this thesis is available in print at TU Wien Bibliothek.

For the PFR to stay in place, it should not be subject to migration. However, all case reports faced migration risk. It has been shown that the devices tend to migrate distally to the right PA [28] [26]. Migration happens as the pressure force acting on the MVP outer surface outperforms the radial force exerted by the device itself. In such a case, the MVP radius loses the friction force and is be transported distally, away from the place where it was implanted.

The analytical model developed by Kizilski et al. (see Appendix B for details), to compute the maximum pressure that the MVP can withstand, avoiding migration, led to Equation 1.4:

$$P_g^{max} = \frac{F_{dev}}{\frac{\pi D^2}{4}\left(\frac{1}{\mu} + \frac{1}{\pi \tan(\theta)} + \frac{2L}{\pi D}\right)}. \tag{1.4}$$

On the numerator, F_{dev} is the radial force that the MVP can exert, whereas the denominator features three terms accounting for the forces acting to knock out of position the device. The first one $(P \times 1/\mu)$[9] is the axial pressure component, characterised by the coefficient of friction μ between the vessel wall and the device, the conical part. The second one $(P \times 1/(\pi \tan(\theta)))$ is the radial pressure component acting on the proximal end of the device. The third one $(P \times 2L/(\pi D))$ is the radial pressure component acting on the cylindrical middle part of the device, allowing paraflow as it compresses the device.

Of note is that the radial expansion force of the MVP decreases as its radius increases when it becomes less compressed [26]. Consequently, the pressure gradient the device can withstand before migrating also diminishes. The primary factor preventing device migration is the friction between the MVP and the vessel wall. If contact is lost migration of the MVP is likely to occur.

1.5 Aim of this project

There remains a gap in the information available for clinicians to make fully informed decisions regarding the use of MVP as a PFR. Mainly, an assessment of its hydraulic characteristics is missing. Kizilsky et al. conducted compressive tests to measure the radial force exerted by the device, but their study used the same plug for multiple experiments, which could have altered

[9] We write $P = 4F_{dev}/(\pi D^2)$.

Die approbierte gedruckte Originalversion dieser Diplomarbeit ist an der TU Wien Bibliothek verfügbar
The approved original version of this thesis is available in print at TU Wien Bibliothek.

the device performances [26]. They also initiated an in vitro setup to assess the pressure drop across the device, but this was limited to only two configurations (MVP with one hole in 5 mm and 8 mm pipes). To better guide decision-makers and optimize the patient-specific use of MVPs as PFRs, additional data across a broader range of configurations is necessary. Our study aimed to address this knowledge gap by investigating how to tailor the hydraulic performance of an MVP to be used as an effective PFR, thereby improving patient outcomes and serving as a reliable bridging tool.

The research was divided into two major characterization approaches: the first involved in vitro experiments and the second focused on in silico simulations. These complementary methods were designed to comprehensively evaluate MVP's hydraulic characteristics. We first assessed the hydraulic resistance of MVPs. We measured the pressure drop across the devices for the three configurations (no, one and two holes), for flow rates up to 2 L/min at steady-state conditions. Additionally, we tested varying pipe diameters and compliances. Afterwards, Computational Fluid Dynamics (CFD) simulations were performed to gain deeper insights into the hemodynamics of the MVP. A washout analysis was conducted to assess hemocompatibility in terms of blood residence time and a thrombus formation risk model was investigated.

Die approbierte gedruckte Originalversion dieser Diplomarbeit ist an der TU Wien Bibliothek verfügbar
The approved original version of this thesis is available in print at TU Wien Bibliothek.

Chapter 2

Materials & Methods

2.1 In Vitro Experimental Analysis

2.1.1 Mock loop set up

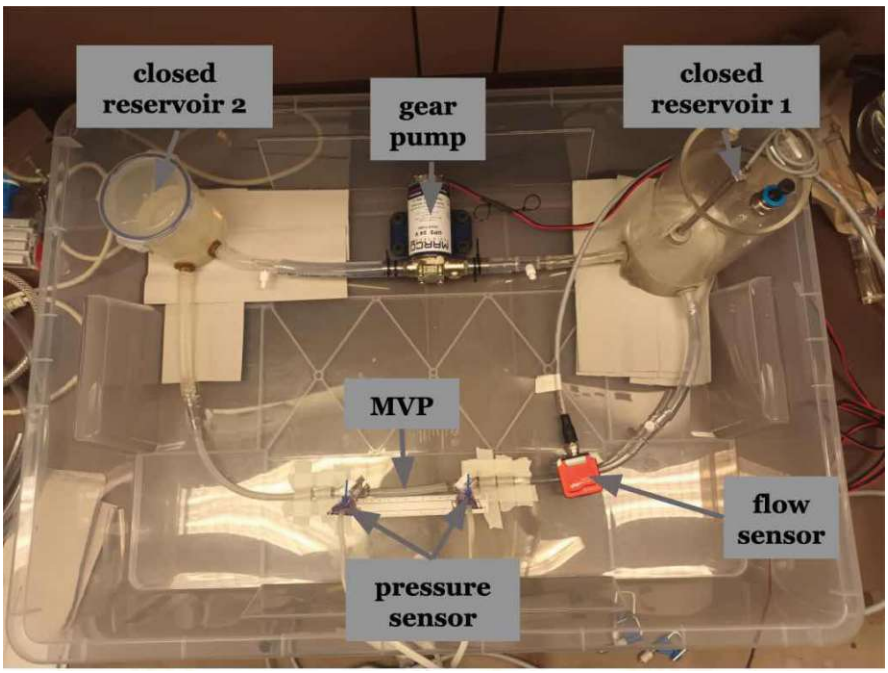

Figure 2.1: *Top view of the MCL set-up. The legends of all its components are added: the gear pump followed by a first reservoir, the flow sensor, the two pressure sensors with the MVP in-between and the second reservoir to close the loop.*

Die approbierte gedruckte Originalversion dieser Diplomarbeit ist an der TU Wien Bibliothek verfügbar
The approved original version of this thesis is available in print at TU Wien Bibliothek.
TU Bibliothek Your knowledge hub WIEN

The hydraulic resistance, or in other terms, the pressure vs. flow rate of the MVP was evaluated in a MCL presented in Figure 2.1 and sketched in Figure 2.2. The flow was measured with a flow sensor (Sonoflow Co.55 - Sonotech GmbH, Halle, Germany) upstream of the MVP placement. The gear pump (UP2 24V - Marco Fluid Tech, Brescia, Italy), responsible for the fluid motion, was controlled by a feedback loop on the flow sensor through the dSpace platform (MicorLabBox, Paderborn, Germany).[1] Pressure drop was measured with two fluid-filled pressure transducers (TruWave - Edwards Lifescience Corp., CA, USA) for flow rates up to 2 L/min with an increment of 0.1 L/min. For each flow rate value, we waited 60 seconds for the pressure drop value to stabilise. We then averaged its value over the last data points ($\simeq$ 20 000 data points). For each experimental configuration, the experiments were repeated four times. All the measurements were performed on the dSpace platform at a sampling rate of 1 kHz.

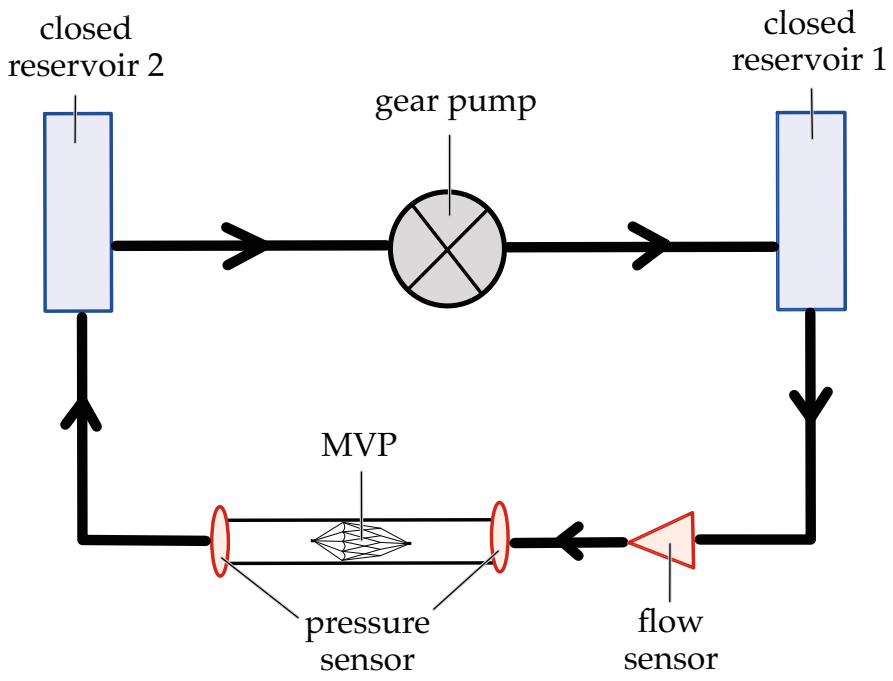

Figure 2.2: *Sketch of the MCL set-up. In blue are the two reservoirs, and in red are the flow and pressure sensors. The arrows explicit the clockwise circulation of the fluid in the loop.*

[1]See Appendix C for details on the loop (Simulink - MathWorks, MA, USA).

Die approbierte gedruckte Originalversion dieser Diplomarbeit ist an der TU Wien Bibliothek verfügbar
The approved original version of this thesis is available in print at TU Wien Bibliothek.

About the pipes

We investigate the MVP hydraulic resistance performance in different pipe diameter sizes and compliances. The goal was to study the influence of these two factors on the hydraulic resistance of the MVP. In Table 2.1, the characteristics of each pipe used are exposed.

Pipe	Diameter size (mm)	Length (cm)	Compliance (qualitative appreciation)
	4.8	9.3	low
	5	9.1	high
	6	9.2	low
	6	9.4	high

Table 2.1: *Pipes characteristics. The two factors of interest are the pipe diameter size and its compliance. The length of the pipes is therefore kept constant (9.25 ± 0.15 cm).*

About the MVP

The medical device of interest is the Medtronic MVP-Q7. The device characteristics are resumed in Table 2.2. It features a nitinol skeleton partially covered by a PTFE membrane, leaving the distal end uncovered (Figure 1.11a). Its intended use for embolisation of peripheral veins makes it a perfect blood flow obstructer. However, we are here interested in regulating the blood flood, a purpose that can be achieved by perforating the PTFE membrane.

The MVP was investigated in three different forms: no hole (unmodified), one hole and two holes (modified). The holes were obtained with an injection needle and expanded by the placement and inflation of a 2 mm balloon

Die approbierte gedruckte Originalversion dieser Diplomarbeit ist an der TU Wien Bibliothek verfügbar
The approved original version of this thesis is available in print at TU Wien Bibliothek.
TU Bibliothek Your knowledge hub WIEN

Product code	MVP-7Q
Recommended vessel size	5.0–7.0 mm
Outer diameter unconstrained	9.2 mm
Length unconstrained	16 mm

Table 2.2: *MVP characteristics.*

catheter. The outcome of a double perforated MVP used for the experiments is shown in Figure 2.3.

Figure 2.3: *Modified MVP featuring 2 holes.*

The MVP was then placed into a pipe and to prevent it from distal migration, two very thin struts (0.3 mm diameter - intended used for acupuncture) were placed in parallel to block the MVP on is distal end (see Figure 2.4). We checked that their contribution to the pressure drop was negligible as their only intended purpose was to avoid migration of the MVP.

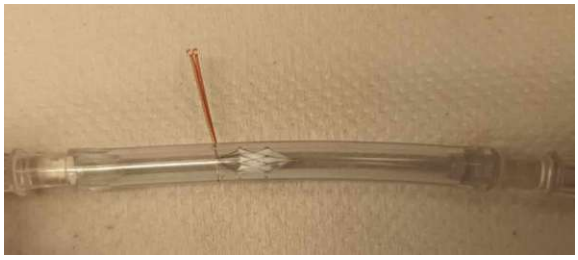

Figure 2.4: *MVP placed in the 4.8 mm diameter pipe with the two struts visible on the left to avoid migration.*

Die approbierte gedruckte Originalversion dieser Diplomarbeit ist an der TU Wien Bibliothek verfügbar
The approved original version of this thesis is available in print at TU Wien Bibliothek.

About the fluid

The fluid used is the literature's classical water-glycerol mixture. To mimic two blood characteristics such as density and viscosity, the adequate water-glycerol ratio was computed [30][31][32]. For a desired haematocrit of 45% (percentage of red blood cells in a blood sample), the required viscosity is 4,6 cP (see Figure 2.5) [30]. For a viscosity of 4.6 cP, a 44.8% glycerol by weight [32] at a temperature of 25°C water-glycerol solution was prepared, which corresponds to a refractive index of 1.39 [31]. The obtained viscosity was checked with an Abbe refractometer (PCE Instruments, Meschede, Germany).

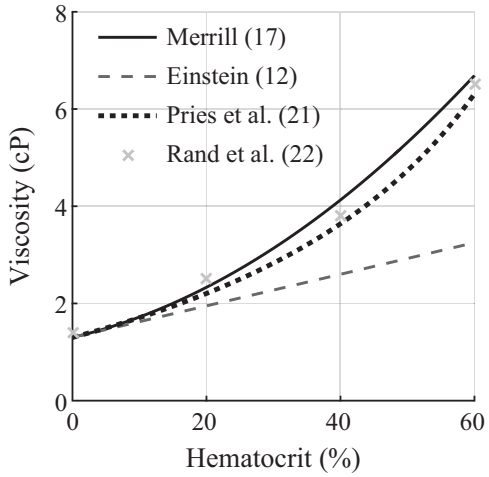

Figure 2.5: *Analytical models of Merrill (17), Einstein (12), Pries et al. (21), and experimental results of Rand et al. (22) for representing the relation of the haematocrit of human blood to viscosity* [30].

2.1.2 Patient-specific geometry extraction

Eventually, we wanted to test the hydraulic performance in a more realistic environment and compare the results with the ones obtained in a straight pipe. Therefore, a HLHS vasculature was cropped from a patient Computed Tomography (CT) scan.

The CT image was imported into Materialize Mimics 24.0 (Materialize, Leuven, Belgium) in the Digital Imaging and Communication in Medicine (DICOM) format. The major vascular vessels - aorta, pulmonary trunk, Right Pulmonary Artery (RPA), Left Pulmonary Artery (LPA) - constituted the segmented anatomical Region of Interest (ROI). Baseline anatomic reference

Die approbierte gedruckte Originalversion dieser Diplomarbeit ist an der TU Wien Bibliothek verfügbar
The approved original version of this thesis is available in print at TU Wien Bibliothek.

measurements for the diameters of the aorta, pulmonary trunk, RPA and LPA were measured and reported in Figure 2.6a. Segmentation of the ROI was performed with a semi-automated threshold tool by selecting the greyscale values of the pixels in the 2D CT image.

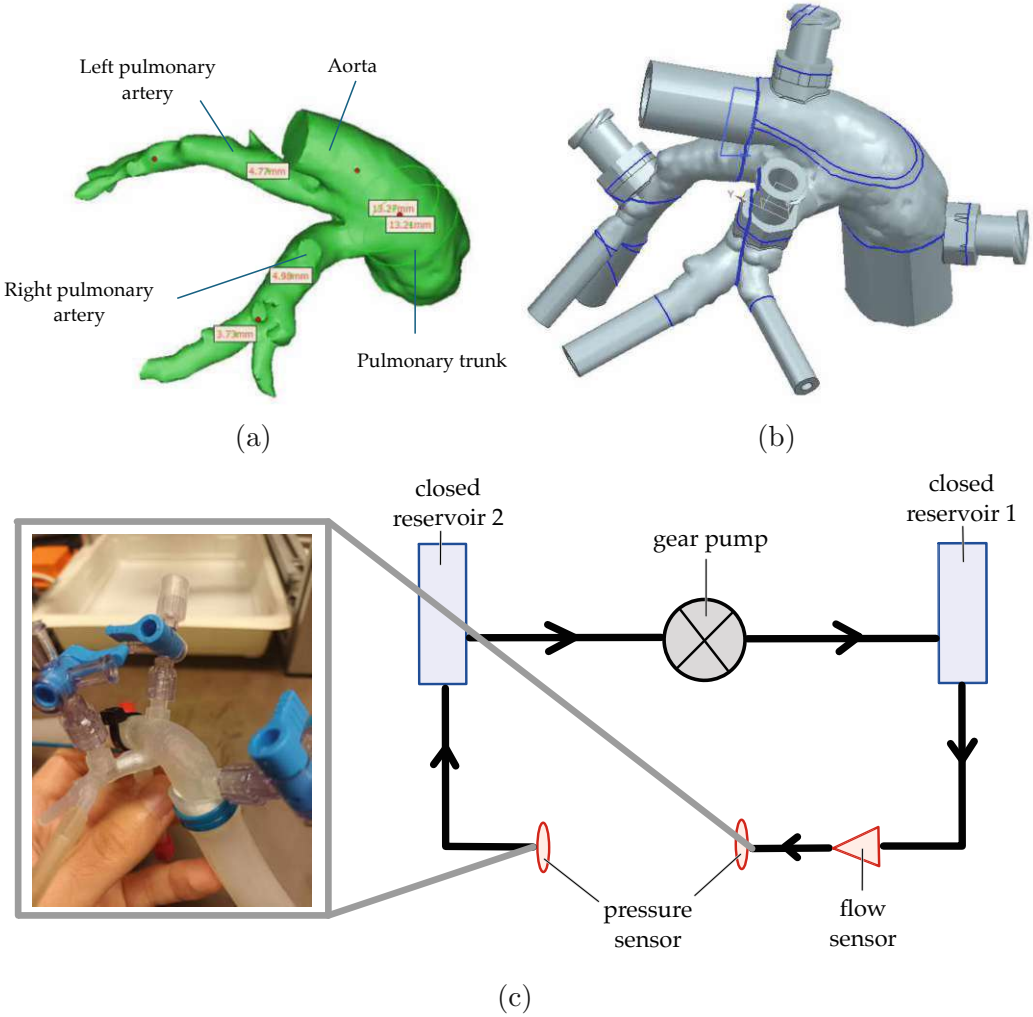

Figure 2.6: *(a) Extracted geometry from patient CT scan with labels and circumferential dimensions of main vessels. (b) Extracted geometry smoothened on NX software with vessel layer growth from the surface outward (1 mm thickness). Additional extensions and luer locks. (c) MVP placement in the RPA and attachment of the printed geometry in a sketched version of the MCL.*

The reconstructed 3D anatomical structure was further processed using a region-growing algorithm to separate and extract the ROI from surrounding

Die approbierte gedruckte Originalversion dieser Diplomarbeit ist an der TU Wien Bibliothek verfügbar
The approved original version of this thesis is available in print at TU Wien Bibliothek.

tissue. Subsequently, the structure was imported into the NX software (Siemens, Munich, Germany) as a stereolithography (.stl) file for additional post-processing to resolve inconsistencies in the 3D anatomical surface model. Its surface was smoothened. Elongations were added - to facilitate the connection of the printed parts to the pipes of the circuit - as well as luer locks connections to enable the attachment of pressure sensors, as can be seen in Figure 2.6b.

The 3D printing was performed out of Clear Resin V4 (Formlabs Inc., Massachusetts, USA). The characteristics of the material used are in Table 2.3.

Ultimate Tensile Strength	65.0 MPa
Tensile Modulus	2.8 GPa
Flexural Modulus	2.2 GPa

Table 2.3: *Clear Resin V4 material properties.*

2.2 In Silico Numerical Analysis

Getting the numerical plug

To perform CFD simulations, a numerical version of the MVP needed to be derived. A 3D version of the plug was reconstructed by reverse engineering out of a full scan of the MVP performed by the SmartSCAN HE-C8 device (Hexagon AG, Stockholm, Sweden). To have the MVP under realistic conditions once placed in the RPA, it was pulled on both sides to stretch it and get

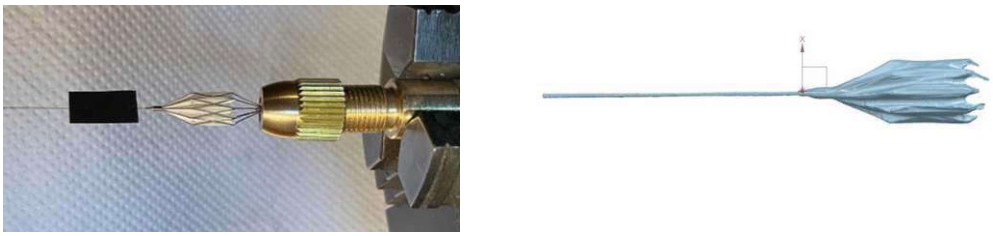

(a) (b)

Figure 2.7: *Set-up for the scan in (a). From left to right: Black tape of 5 mm width, stretched MVP and fixation support. The black tape is 5 mm wide to indicate the matching size of the MVP diameter. A 3D reconstructed scan visualized on NX is in (b).*

Die approbierte gedruckte Originalversion dieser Diplomarbeit ist an der TU Wien Bibliothek verfügbar
The approved original version of this thesis is available in print at TU Wien Bibliothek.
TU Bibliothek Your knowledge hub WIEN

its diameter from 9.2 mm (unconstrained state) to 5 mm (see Figure 2.7a). As the camera could not go around the device because of the pulling structures, the device itself was rotated along its longitudinal axis. This was done to have a fully 3D reconstruction of the MVP (see Figure 2.7b).

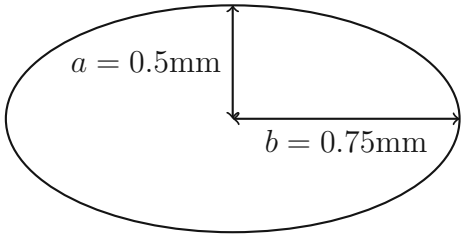

Figure 2.8: *Elliptical shape for MVP's perforation(s). Half-length of the minor and major axes are displayed as a and b respectively.*

In the Computer-Aided Design (CAD) software NX (Siemens AG, Munich, Germany), the numerical MVP was refined, and some modifications were made. The proximal filament was cut out and holes were added. To replicate the holes clinicians have defined on the PTFE membrane of MVP, we opted for an elliptical shape, as the numerical MVP was already in a constricted modified state compared to the unconstricted initial state. The ellipse's major and minor axes lengths are displayed in Figure 2.8. They were chosen to replicate as closely as possible the size of the perforations performed by the clinicians for the in vitro experiments.

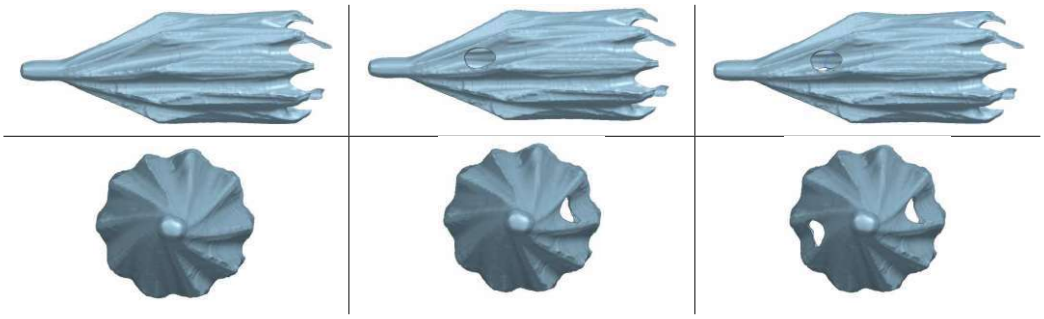

Table 2.4: *Side (top) and frontal (bottom) NX software rendering of the three versions of the MVP that are used in the numerical simulations. The tilting of the MVP during the scanning process is visible from the frontal view, in which the nitinol wires do not point straight towards the centre but are slightly curved.*

Die approbierte gedruckte Originalversion dieser Diplomarbeit ist an der TU Wien Bibliothek verfügbar
The approved original version of this thesis is available in print at TU Wien Bibliothek.

The three different versions of the MVP used in the simulations are shown in Table 2.4. The MVP was then embedded in a 10 cm long diameter pipe (see Figure 2.9). Ideally, the pipe had a diameter of 5 mm as we wanted to compare it to the in vitro experiment set-up. However, the tilting that occurred during the scan did not allow accurate length maintenance and the MVP radius resulted slightly greater (14%) than the 5 mm target. To still fit it in the fluid cylindrical region without touching the surface, this one was chosen to be 5.75 mm in diameter.

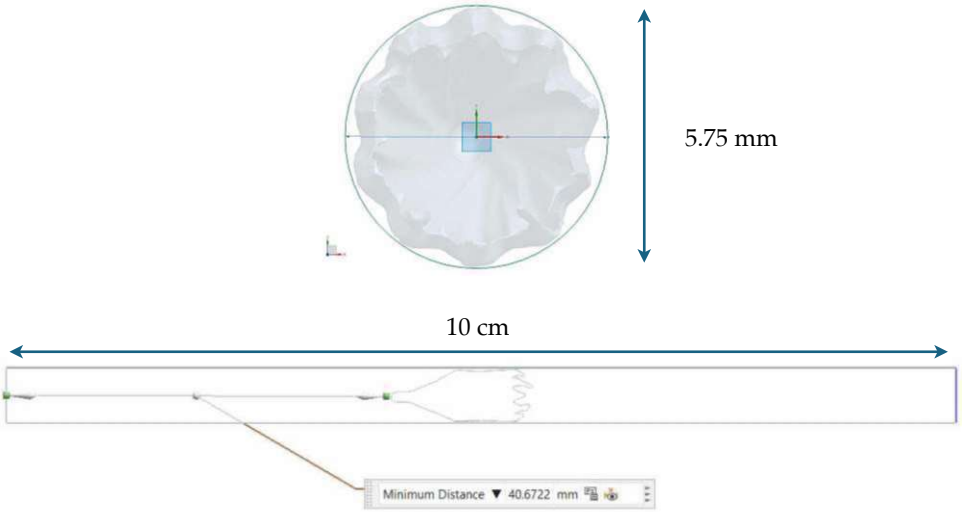

Figure 2.9: *Dimensions of the MVP and cylinder to define the fluid region with CAD NX software.*

2.2.1 Simulation set up

Mesh

The mesh generation step is an essential and critical step for a successful simulation. It corresponds to the discretization of the spatial computational domain. The fluid region was meshed with Star CCM+ software (Siemens AG, Munich, Germany), using a hex-core mesh (see Figure 2.11) and prism layers in the near-wall region.

The mesh outcome is resumed in Table 2.5. A mesh independence study was conducted. This was to make sure that the reached solution was independent of the number of mesh elements. Too few elements may lead to an inaccurate solution, whereas too many may require very expensive

Die approbierte gedruckte Originalversion dieser Diplomarbeit ist an der TU Wien Bibliothek verfügbar
The approved original version of this thesis is available in print at TU Wien Bibliothek.

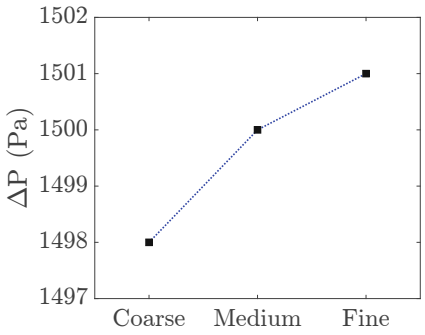

Figure 2.10: *Mesh independence analysis for MVP with No Hole at $Q = 0.1$ L/min.*

computing power. The mesh-independent study is there to find the right number of elements that balance out these two factors. The converged value of the pressure drop between the outlet and the inlet was used as a metric of comparison. The results in Figure 2.10 indicated a mesh element number of about 4.4 million elements for the fluid region.

		No hole	**1 hole**	**2 holes**
Mesh (millions)	**cells**	4.4	5.1	5.0
	faces	13.0	15.0	14.9
	verts	4.6	5.2	5.2
Mesh Quality (number of bad cells)	**face validity**	3	0	0
	cell quality	0	0	0
	volume change	5	9	5
	cell skewness	20	36	32
	angle			
y^+ **Value**	**maximum value**	0.9	1.9	1.7
	number of cells above 1	0	17	17

Table 2.5: *Mesh Quality Assessment table at inflow rate of $Q = 0.1$ L/min. MVPs mesh cells, mesh quality and y^+ value.*

The y^+ value appearing in Table 2.5 is a dimensionless quantity used to evaluate mesh resolution at near-wall regions, especially for turbulent flow simulations [33]. Its physical definition is:

$$y^+ = \frac{\rho u_\tau y}{\mu} \tag{2.1}$$

with:

Die approbierte gedruckte Originalversion dieser Diplomarbeit ist an der TU Wien Bibliothek verfügbar
The approved original version of this thesis is available in print at TU Wien Bibliothek.

- ρ: the fluid density;
- μ: the fluid viscosity;
- y: the distance from the wall to the first grid point;
- u_τ: the velocity friction at the wall, defined as $u_\tau = \sqrt{\frac{\tau_w}{\rho}}$, τ_w being the wall shear stress.

Its value helps determine whether the mesh is fine enough to capture the physics of the near-wall flow. To be able to resolve the viscous very thin sublayer, y^+ should be smaller than 1, or not much greater [33].

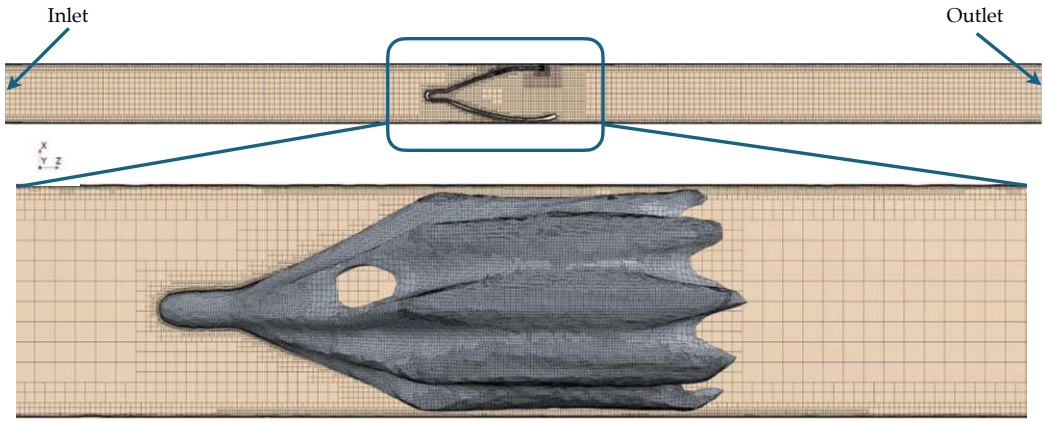

Figure 2.11: *Mesh outcome.*

Physical model

A Newtonian blood model, with a density of 1117.5 kg/m^{-3}, corresponding to the target haematocrit of 45%, and a constant viscosity of 4.6 cP was used. As a turbulent model, we opted for the $k-\omega$ shear stress transport model. It is a model based on two transport equations: the turbulent kinetic energy (k) and the dissipation rate of the kinetic energy (ω). This model is specifically relevant when solving for the near-wall regions between the surface of the MVP and the pipe wall.

The simulation was divided into two stages. The first one, was for haemodynamics, solving for the velocity and pressure fields, among other relevant quantities (wall shear stress, stagnation zone), and the second one was for the thrombus formation risk model.

Die approbierte gedruckte Originalversion dieser Diplomarbeit ist an der TU Wien Bibliothek verfügbar
The approved original version of this thesis is available in print at TU Wien Bibliothek.

For the first stage simulation for haemodynamics, a time step of 0.1 ms was applied, and the stabilisation of the pressure difference between the inlet and the outlet was used as a termination criterion. For the second stage simulation - for the thrombus formation risk that we will discuss immediately -, a time step of 1 s was applied and the stabilisation of the volume-average value of the Active Platelets (AP) concentration in the fluid domain was used as a termination criterion.

2.3 Washout with the passive scalar approach

A washout analysis was conducted by looking at how, and how much time, it took for a "new blood" fluid volume to replace an "old blood" fluid volume in the entire domain of consideration. We did so with the help of a passive scalar. A passive scalar is a scalar quantity that is governed by a scalar transport equation, similar to the Navier-Stokes equations[2] of momentum, but without depending on them. In simple terms, it is a scalar quantity that interacts with the fluid properties without affecting them. Taking a snapshot of the passive scalar every 20 iterations allowed for visualisation of the haemodynamics during the process.

All the cells were set to 1 (old blood) in the entire domain. As new blood got into the fluid domain at the inlet, all the cell values decreased progressively, eventually getting to 0 (new blood), revealing the end of the washout.

Time step considerations

The washout was performed for $Q = 0.4$ L/min $= 6.67.10^{-5} m^3/s$, $R = 2.875.10^{-3}$ m and we wanted to solve the equations every 2 mm, therefore: $\Delta x = 2.10^{-3} m$.

$$\Delta t = \frac{\Delta x}{< v >} = \frac{\Delta x \pi R^2}{Q}$$

$$\Delta t = 0.00078\ s \approx 1\ ms$$

with $< v >$ the velocity mean value, 20 steps are performed for 1 cycle and the simulation runs for 1000 time steps.

[2]The Navier-Stokes equations are the equations that govern fluid motion. They are the fundamental equations of fluid dynamics.

Die approbierte gedruckte Originalversion dieser Diplomarbeit ist an der TU Wien Bibliothek verfügbar
The approved original version of this thesis is available in print at TU Wien Bibliothek.

2.4 Thrombus Formation Risk Model

Thrombosis is when a blood clot, a thrombus, forms and blocks blood circulation in veins and/or arteries. Before digging into the thrombus formation model, it is important to get familiar with the Virchow's triad and its implications.

2.4.1 The Virchow's triad

We just discussed the washout analysis. As it reveals how much time it takes for blood to be washed out, it also informs us about the blood residence time and the risk of blood stagnation. Blood stagnation is particularly important when it comes to thrombus formation risk, as it is one of the three factors contributing to it. Together with two other factors, that we will briefly mention immediately after, we can form what is called the Virchow's triad (see Figure 2.12).

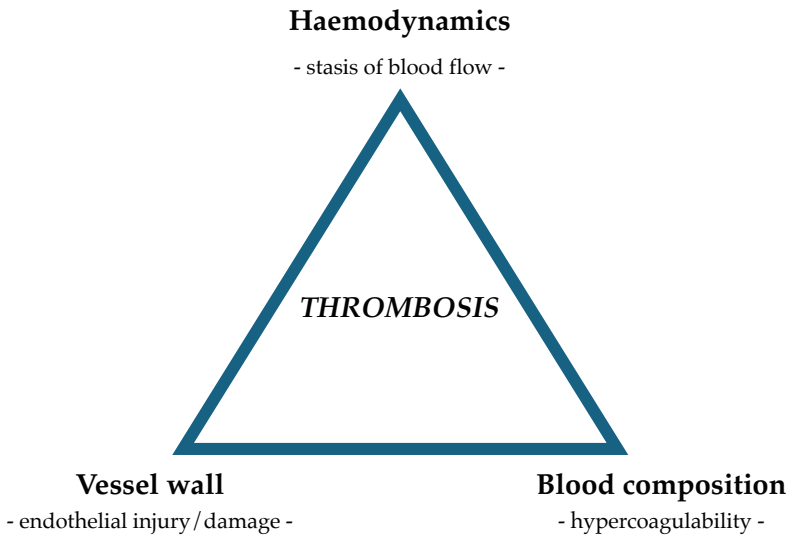

Figure 2.12: *Virchow's Triad and the contribution of the three factors to thrombus risk formation.*

The Virchow's triad is a simple representation of the overall knowledge, or perhaps the lack of knowledge, we encounter when facing thrombus formation risk. Along with haemodynamics, the two other corners of the triangle are

Die approbierte gedruckte Originalversion dieser Diplomarbeit ist an der TU Wien Bibliothek verfügbar
The approved original version of this thesis is available in print at TU Wien Bibliothek.

completed with vessel wall damage and blood composition. These are the three major factors contributing to thrombus formation. It is easy to imagine that for a person with a blood composition high in coagulates, her or his blood will have a stronger tendency to coagulate and therefore to form a thrombus.

Encountering one, two, or three of these three factors can lead to a thrombus formation. However, in which proportions are they responsible for it, it is yet to be understood. This is a very important aspect to bear in mind. So far, there is no consensus among the scientific community on how much of a combination of the three features is enough to start the cascade of thrombus formation, the so-called coagulation cascade.

In our study, the presence of a foreign object, the MVP, alters flow characteristics, potentially increasing the risk of thrombus formation. Therefore, we aimed to develop a thrombus formation risk model that primarily considers blood hemodynamics —establishing velocity and pressure fields first— and incorporates blood composition then, by accounting in terms of platelets and platelet activation. The third element of the Virchow's triad, endothelial injury, was not included in this model.

2.4.2 The Model

The implementation of the model mostly relied on Blum et al. work [34]. In this thrombus model, the focus was set on the platelets' activation. Platelets are blood components that aggregate to form clots when activated. We looked at three different species: AP, Non-active Platelets (NP) and Adenosine Diphosphate (ADP), whose respective concentrations Φ_a, Φ_n and ADP are governed by the following three transport convection-diffusion equations.

$$\frac{\partial \Phi_a}{\partial t} + \underbrace{(\mathbf{u}.\nabla)\Phi_a}_{\text{convection}} = \underbrace{D_a \nabla^2 \Phi_a}_{\text{diffusion}} + \underbrace{\{[A_c(ADP)]\Phi_n + [A_m(\Phi_f, \tau)](\Phi_a + \Phi_n)\}}_{\text{source term}} \quad (2.2)$$

$$\frac{\partial \Phi_n}{\partial t} + (\mathbf{u}.\nabla)\Phi_n = D_n \nabla^2 \Phi_n - \{[A_c(ADP)]\Phi_n + [A_m(\Phi_f, \tau)](\Phi_a + \Phi_n)\} \quad (2.3)$$

$$\frac{\partial ADP}{\partial t} + (\mathbf{u}.\nabla)ADP = D_{ADP} \nabla^2 \Phi_{ADP} + R_{ADP}\{[A_c(ADP)]\Phi_n + [A_m(\Phi_f, \tau)](\Phi_a + \Phi_n)\} \quad (2.4)$$

Die approbierte gedruckte Originalversion dieser Diplomarbeit ist an der TU Wien Bibliothek verfügbar
The approved original version of this thesis is available in print at TU Wien Bibliothek.
TU Bibliothek Your knowledge hub WIEN

Each of the equations features a convective, diffusion and source term (see Equation 2.2). D_x are the respective diffusivity coefficients of each of the three species. Two aspects come into play in terms of activation of the platelets in the source terms. There is the mechanical activation $A_m(\Phi_f, \tau)$ depending on the ratio of activated platelet to total platelets count $\Phi_f = \Phi_a/(\Phi_a + \Phi_n)$ and the scalar shear stress τ, and a chemical activation depending on the ADP concentration. Both activations are defined as follows:

$$A_m(\Phi_f, \tau) = (1 - \Phi_f) C^{\frac{1}{\beta}} \beta \Phi_f^{\frac{1-\beta}{\beta}} \tau^{\frac{\alpha}{\beta}} \tag{2.5}$$

$$A_c(ADP) = \begin{cases} \frac{ADP}{ADP_t \ t_{ADP}} & ADP \geq ADP_t, \\ 0 & ADP < ADP_t. \end{cases} \tag{2.6}$$

For the mechanical activation, C, α and β are the parameters of the power law model from [35] and the scalar shear stress τ is calculated according to Equation 2.7 in which the σ_{ij} are the shear stress tensor components.

$$\tau = \frac{1}{\sqrt{3}} \sqrt{\sigma_{xx}^2 + \sigma_{yy}^2 + \sigma_{zz}^2 - \sigma_{xx}\sigma_{yy} - \sigma_{xx}\sigma_{zz} - \sigma_{yy}\sigma_{zz} + 3(\sigma_{xy}^2 + \sigma_{xz}^2 + \sigma_{yz}^2)} \tag{2.7}$$

As for the chemical activation, ADP_t is the threshold for chemical activation (must be reached before any activation process starts) and t_{ADP} is the characteristic time of platelet activation rate.

Note that the source terms for AP and NP differ only by the sign. This is to ensure mass conservation in the platelet population. Platelets that are activated come from platelets that were not activated the moment before.

Regarding Equation 2.4 for ADP, the only production term is due to the release of ADP by AP. The rate of ADP release is therefore calculated by multiplying the amount of ADP contained in a platelet, R_{ADP}, by the rate of platelet activation $\{[A_c(ADP)]\Phi_n + [A_m(\Phi_f, \tau)](\Phi_a + \Phi_n)\}$ [36].

In order to implement the model into Star CCM+, we defined for each species a passive scalar in which transport governed by both convection and diffusion was enabled. All the three passive scalar were kept frozen during the first part of the simulation for the computation of velocity and pressure fields. They were activated once the first simulation was completed. For further details on the translation of the equations into the software, please refer to Appendix D.

Die approbierte gedruckte Originalversion dieser Diplomarbeit ist an der TU Wien Bibliothek verfügbar
The approved original version of this thesis is available in print at TU Wien Bibliothek.
TU Bibliothek Your knowledge hub WIEN

Variable	Definition	Initial Value
D_a	Diffusion coefficient for activated platelets	1.58e-11 ($m^2.s^{-1}$)
D_n	Diffusion coefficient for non-activated platelets	1.58e-11 ($m^2.s^{-1}$)
D_{ADP}	Diffusion coefficient for ADP	1e-20 ($m^2.s^-1$)
R_{ADP}	Amount of ADP released during one platelet activation	3e-17 (mol)
ADP_t	Threshold value for activation of platelets	2e-3 ($mol.m^{-3}$)
t_{ADP}	Characteristic time of platelet activation rate	1 (s)
C		1.4854e-7
α	Coefficients of power law model	1.4854
β		1.4401
ϕ_a	Concentration of activated platelets	25e12 (m^{-3})
ϕ_b	Concentration of non-activated platelets	475e12 (m^{-3})

Table 2.6: *Parameters involved in the thrombosis risk model taken from Blum et al.* [34].

In Table 2.6 are resumed all the constants values used in the simulation. In the model we put in place, the hemodynamics aspect is enfolded in the three transport equations, figuring a convection and diffusion term along the source terms (mechanical and chemical activation), whereas the blood composition is encased in the three considered species: AP, NP and ADP. As a thrombus formation risk region, we looked at the regions in the fluid domain where the increase of concentration of AP reaches a certain threshold.

2.5 Paraflow and flow through an orifice

One of the major questions related to the modified MVP used as PFR is how much of the fluid, in this case blood, flows through the hole(s) at a given pressure. To avoid migration, the radial force produced by the device should be strong enough to prevent any paraflow. In such case, the fluid has no other options than to flow through the holes.

There is an analytical formulation demonstrating that the pressure drop and the flow rates have a quadratic dependency when fluid flows through a hole:

Die approbierte gedruckte Originalversion dieser Diplomarbeit ist an der TU Wien Bibliothek verfügbar
The approved original version of this thesis is available in print at TU Wien Bibliothek.

$$\Delta P \propto Q^2.$$

The goal of the following section is to retrieve this dependency to compare the analytical formula to the in vitro experiments.

Pressure-Flow relationship for flow through an orifice

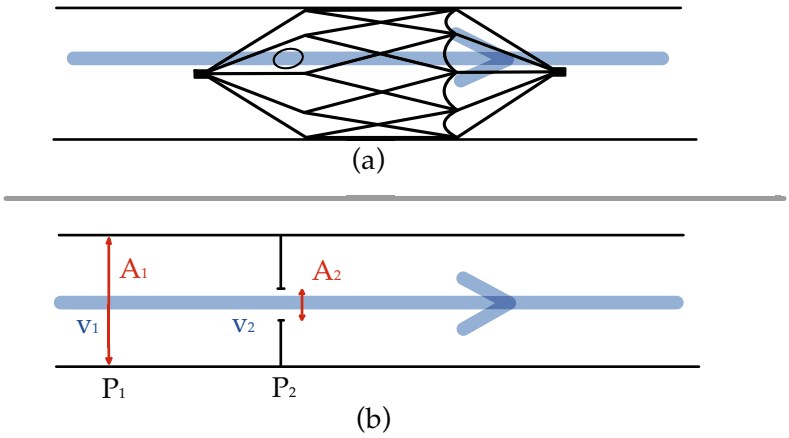

Figure 2.13: *Sketches of MVP (a) and analogy with flow through a circular orifice (b). The fluid line used to explicit the Bernoulli equation is represented in blue. The problem's parameters are displayed as well with P_i the pressures, v_i the velocities and A_i the cross-sectional areas.*

We start with the very well-known Bernoulli equation established along a fluid line that passes through the hole (see Figure 2.13). In the traditional application of Bernoulli's theorem, fluid flow is analysed through a conduit with a continuously varying cross-section. In this specific case, however, the change in cross-section is sudden and localized because of the hole. Therefore, it is necessary to introduce a term to account for it: the kinetic losses.

$$\frac{P_1}{\rho} + \frac{1}{2}v_1^2 = \frac{P_2}{\rho} + \frac{1}{2}v_2^2 + \underbrace{K_L}_{\text{kinetic losses}} . \tag{2.8}$$

Considering the mass conservation equation:

$$v_1 A_1 = v_2 A_2 = Q, \tag{2.9}$$

Die approbierte gedruckte Originalversion dieser Diplomarbeit ist an der TU Wien Bibliothek verfügbar
The approved original version of this thesis is available in print at TU Wien Bibliothek.

where A_1 is the cross-sectional area of the pipe and A_2 is the cross-section area of the orifice, we can write 2.8 differently:

$$\frac{P_1 - P_2}{\rho} = \frac{1}{2}Q^2 \frac{1}{A_2^2}\left[1 - \left(\frac{A_2}{A_1}\right)^2\right] + K_L.$$

We note $\Delta P = P_1 - P_2$ and we explicit the kinetic losses term as:

$$K_L = \frac{1}{2}kv_2^2,$$

where $k = \beta\left[1 - \left(\frac{A_2}{A_1}\right)^2\right]$, with β a constant. Further rearrangement of terms leads to:

$$Q = C_d A_2 \sqrt{\frac{2\Delta P}{\left[1 - (A_2/A_1)^2\right]\rho}},$$

where C_d is the discharge coefficient.[3] From empirical observation, we have $C_d = 0.62$ [37]. In order to have the pressure drop as a function of the flow rate, we can simply write:

$$\Delta P = \alpha Q^2 \tag{2.10}$$

with

$$\alpha = \frac{\left[1 - (A_2/A_1)^2\right]\rho}{2C_d^2 A_2^2}. \tag{2.11}$$

[3] C_d can be expressed as a function of β: $C_d = 1/\sqrt{1+\beta}$.

Die approbierte gedruckte Originalversion dieser Diplomarbeit ist an der TU Wien Bibliothek verfügbar
The approved original version of this thesis is available in print at TU Wien Bibliothek.

Chapter 3

Results

3.1 In Vitro Experimental Results

Our goal was to assess the hydraulic characteristic of the MVP under different configurations: unmodified MVP, MVP with one hole and MVP with two holes. The Pressure-Flow curves in different experimental set-up were measured in order to compare relevant behaviours of the three versions of the

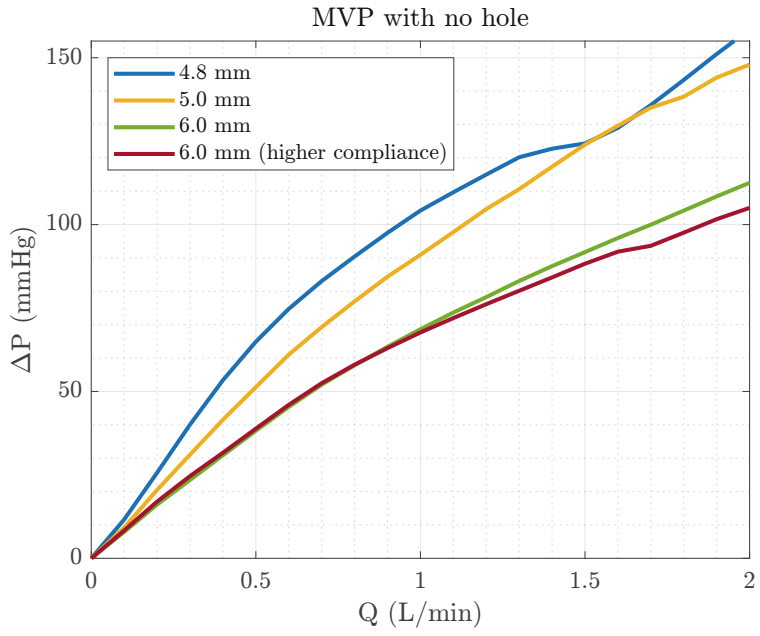

Figure 3.1: *Average pressure drop curves for four samples across unmodified MVP for flow rates ranging from 0 to 2 L/min. Influence of pipe diameter size and compliance.*

Die approbierte gedruckte Originalversion dieser Diplomarbeit ist an der TU Wien Bibliothek verfügbar
The approved original version of this thesis is available in print at TU Wien Bibliothek.

MVP from a hydraulic perspective. In Figure 3.1, the Pressure-Flow curves for the unmodified MVP are plotted.

The first thing to note is a non-linear increase in the pressure difference with the flow rate. In general, the smaller the pipe diameter, the higher the pressure drop. The pressure difference is higher in the 4.8 mm diameter pipe than in the 5.0 mm diameter pipe, which in turn, is higher than the pressure in the two 6.0 mm diameter pipes. For these latest two, the pressure drop is overall higher in the less compliant pipe, especially at high flow rates.

In all four pipes, the pressure increases sharply and then slows down. Focusing on the different sizes of the pipe diameters, the 4.8 mm and 5.0 mm diameter pipes have very similar behaviour (Root Mean Square Error (RMSE) = 9.5 mmHg). The same can be said for the two 6.0 mm diameter pipes (RMSE = 3.4 mmHg), for which the only thing that distinguishes them is the compliance. The gap between these two groups (one with the 4.8 mm and

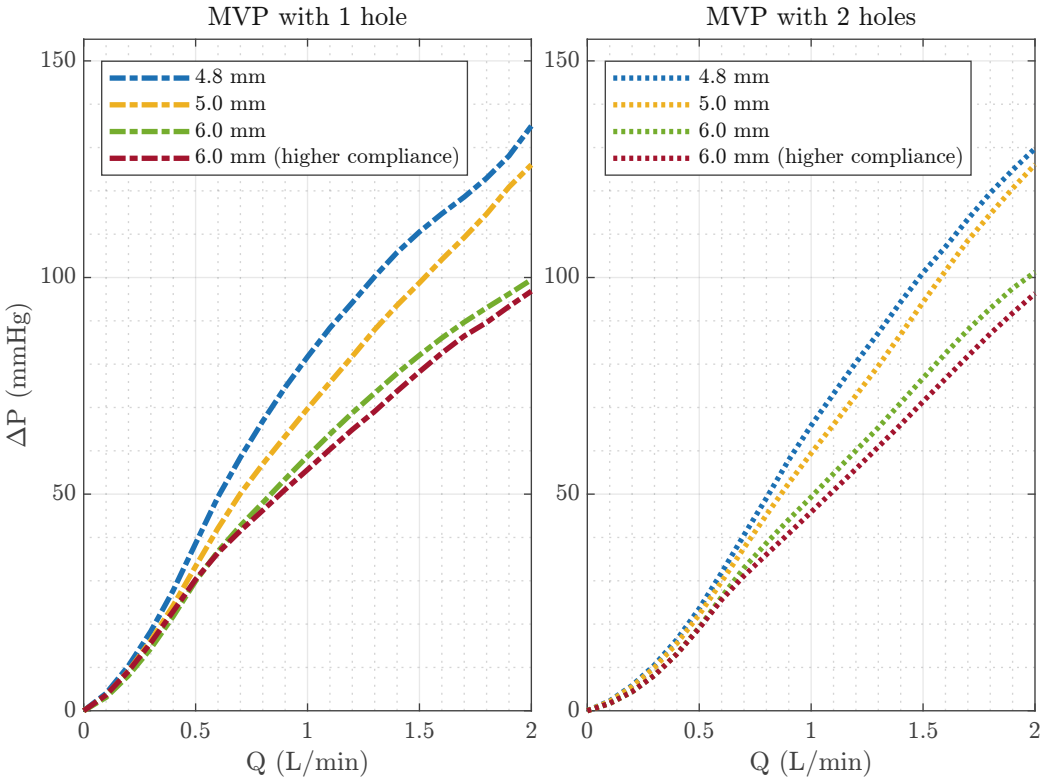

Figure 3.2: *Average pressure drop curves for four samples across MVP with one hole (left) and MVP with two holes (right) for flow rates ranging from 0 to 2 L/min. Influence of pipe diameter size and compliance.*

Die approbierte gedruckte Originalversion dieser Diplomarbeit ist an der TU Wien Bibliothek verfügbar
The approved original version of this thesis is available in print at TU Wien Bibliothek.

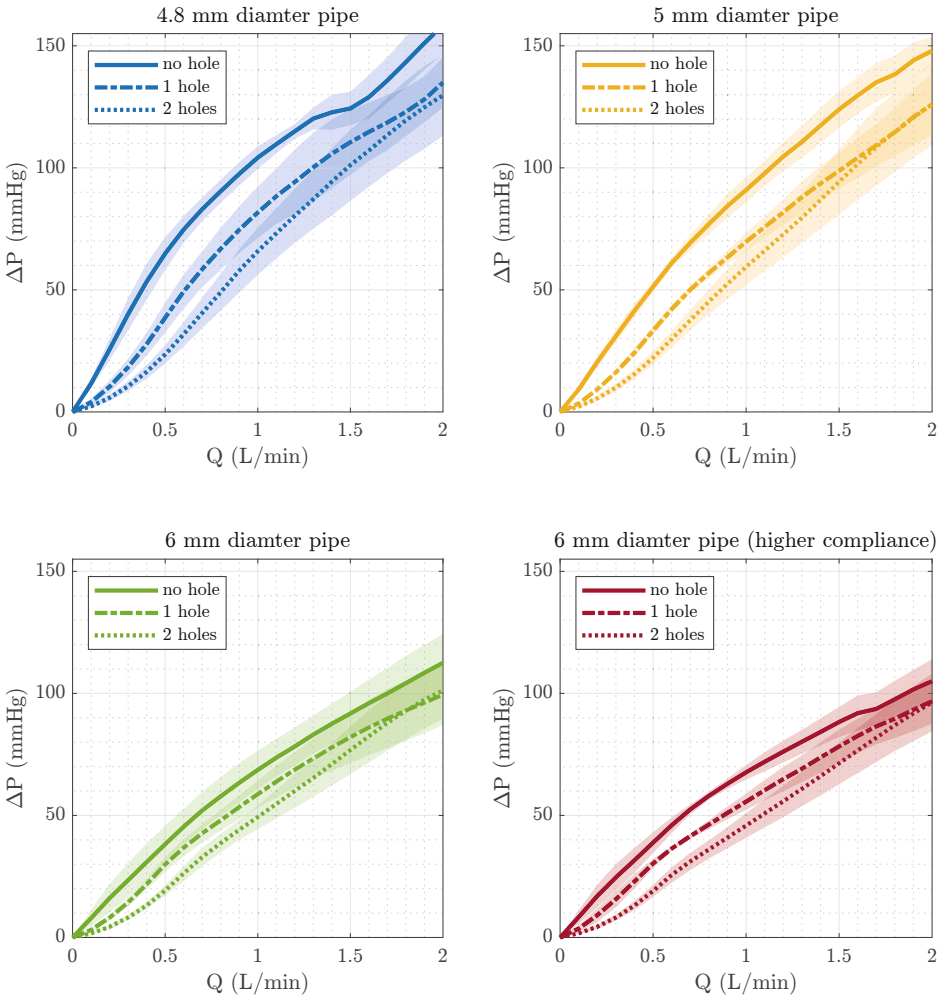

Figure 3.3: *Average pressure drop curves for four samples across different vessel diameters and compliance for flow rates ranging from 0 to 2 L/min. The shaded regions represent standard deviation for four samples. Influence of perforation choice.*

5.0 mm pipes, and the other with the two 6 mm pipes) is always there but digs deeper at high flow rates. Considering the 4.8 mm diameter pipe and the low-compliance 6 mm pipe, at low flow rates (up to 0.4 L/min): RMSE = 13 mmHg, and at high flow rates (above 1.5 L/min): RMSE = 39 mmHg.

In Figure 3.2 are plotted the results for the MVP with one and two holes. In both cases, the relationship at low flow rates is different compared to the no hole configuration. The initial increase of the pressure drop seems to be quadratic for both configurations. Moreover, there is almost no distinction

Die approbierte gedruckte Originalversion dieser Diplomarbeit ist an der TU Wien Bibliothek verfügbar
The approved original version of this thesis is available in print at TU Wien Bibliothek.

between the four pipes at low flow rates, whereas at high flow rates, the difference between the two smaller pipes and the 6 mm diameter pipes is important. Comparing the 4.8 mm diameter pipe (blue curve in Figure 3.2) and the 6 mm diameter higher compliance pipe (red curve in Figure 3.2), we get at low flow rates (up to 0.4 L/min) RMSE = 2.5 mmHg and at high flow rates (above 1.5 L/min) RMSE = 34 mmHg for 1 hole, and RMSE = 2.0 mmHg at low flow rates and RMSE = 32 mmHg at high flow rates for 2 holes.

So far, the way the graphs are build allows to see the effect on pipe diameter size and compliance. The graphs in Figure 3.3 are especially useful for appreciating the results from the same dataset, but this time in terms of the influence of the perforation choice. For each of the four pipes, similar patterns are visible: (1) for the same flow rate, the MVP with no holes exhibits always the higher pressure drop, followed by the MVP with one hole and the MVP with no hole; (2) for the one and two holes configurations, at low flow rates, up to 0.4 L/min, the relationship between the pressure drop and the flow rate seems to be quadratic; (3) at high flow rates, above 1.5 L/min, the pressure drop for the MVP with one and two hole(s) converge to a same value.

3D patient geometry

About the experiment in the patient specific geometry, the results are shown in Figure 3.4. The pressure drop in the 3D-printed geometry is compared to the one measured for the MVP with two holes in the 5 mm diameter pipe. The quadratic dependency at low flow rates is captured as well in this case and the RMSE = 2.9 mmHg value reflects the similarity of the results obtained for the two measurements.

3.1.1 Analytical Results

To be able to compare the analytical solution with the experimental plots, there are two more considerations to take into account. The first one is about dimensional analysis. The analytical reasoning that led to the formulation of Equation 2.10 was conducted in SI units[1]. Therefore, as it stands, α is in $\frac{\text{Pa}}{(\text{m}^3/\text{s})^2}$. However, to have comparable results we need it in $\frac{\text{mmHg}}{(\text{L/m})^2}$, so a coefficient c must be added:

$$c = \frac{1/133.3}{60000^2}.$$

[1]from French *Système International d'unités*, International System of Units

Die approbierte gedruckte Originalversion dieser Diplomarbeit ist an der TU Wien Bibliothek verfügbar
The approved original version of this thesis is available in print at TU Wien Bibliothek.

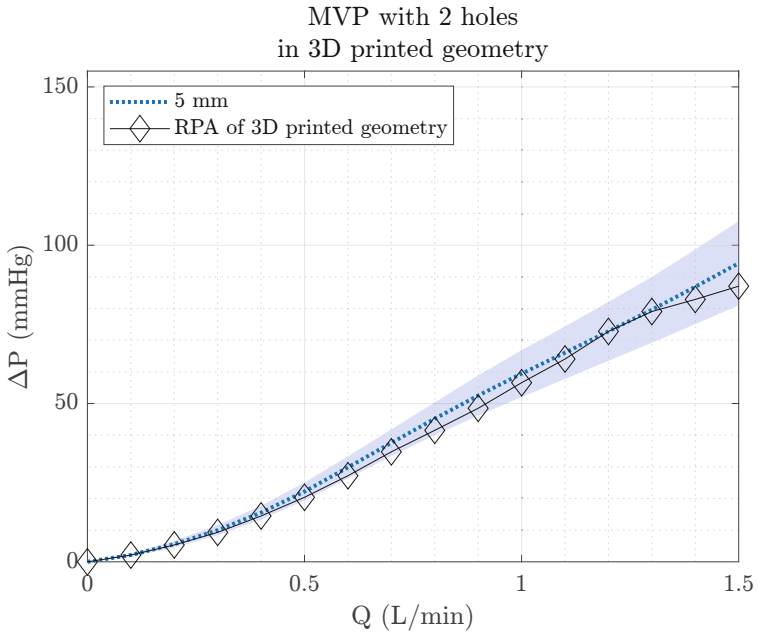

Figure 3.4: *Pressure-flow curve for the 3D-printed geometry. Comparison with pressure-flow curve in the case of the MVP in the 5 mm diameter pipe.*

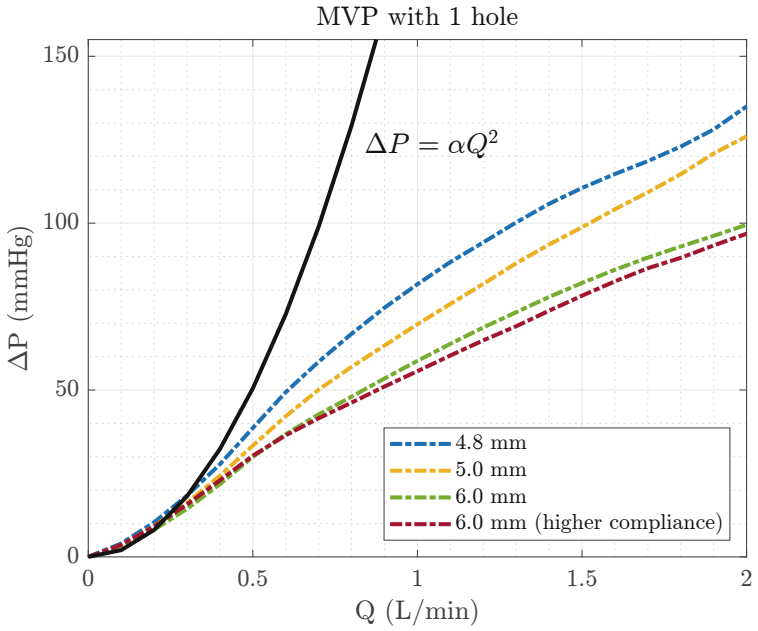

Figure 3.5: *Comparison of the analytical formula, plotted in dark, with the in vitro experiments for the MVP with one hole.*

Die approbierte gedruckte Originalversion dieser Diplomarbeit ist an der TU Wien Bibliothek verfügbar
The approved original version of this thesis is available in print at TU Wien Bibliothek.

The second consideration is about the value for the cross-sectional orifice area A_2 that should be taken for the numerical application. As best fitting outcome, we choose the orifice's radius equal to 1.1 mm. We used it to compute the value of A_2 and inserted it in Equation 2.11. Multiplying by the factor c, we get the value for α

$$\alpha = \frac{\left(\left(1 - \left(\frac{\pi\left(1.1\times10^{-3}\right)^2}{\pi(2.5\times10^{-3})^2}\right)^2\right) \times 1117.5\right)}{2 \times 0.62^2 \times \left(\pi\left(1.1 \times 10^{-3}\right)^2\right)^2} \times \frac{1/133.3}{60000^2}$$

$$\alpha \approx 202 \left[\frac{\text{mmHg}}{(\text{L/m})^2}\right]. \tag{3.1}$$

The plot of the analytical formula together with the Pressure-Flow curves obtained experimentally is shown in Figure 3.5. At low flow rates, ranging from 0 to 0.4 L/min, a good fitting of the analytical results to the experimental ones can be observed (RMSE = 3.8 mmHg).[2]

MVP's size reduction

The following image series was taken during experiments with the MVP with two holes, conducted in the low-compliance, 6 mm diameter pipe. The images illustrate the reduction in the proximal diameter of the MVP with increasing flow rate.

We used these pictures to measure the proximal diameter change with increasing flow rate with the use of an image analysis software (Roduit, N. JMicroVision: Image analysis toolbox for measuring and quantifying components of high-definition images. Version 1.3.1). The decrease in the MVP radius - a 25% decrease at 2 L/min - with increasing flow rate is shown in Figure 3.8.

[2]The comparison was made with the experiments conducted on the MVP with one hole in the 5 mm diameter pipe.

Die approbierte gedruckte Originalversion dieser Diplomarbeit ist an der TU Wien Bibliothek verfügbar
The approved original version of this thesis is available in print at TU Wien Bibliothek.

$Q = 0.1$ L/min

$Q = 0.2$ L/min

$Q = 0.3$ L/min

$Q = 0.4$ L/min

$Q = 0.5$ L/min

$Q = 0.6$ L/min

$Q = 0.7$ L/min

$Q = 0.8$ L/min

$Q = 0.9$ L/min

$Q = 1.0$ L/min

$Q = 1.1$ L/min

$Q = 1.2$ L/min

$Q = 1.3$ L/min

$Q = 1.4$ L/min

Die approbierte gedruckte Originalversion dieser Diplomarbeit ist an der TU Wien Bibliothek verfügbar
The approved original version of this thesis is available in print at TU Wien Bibliothek.

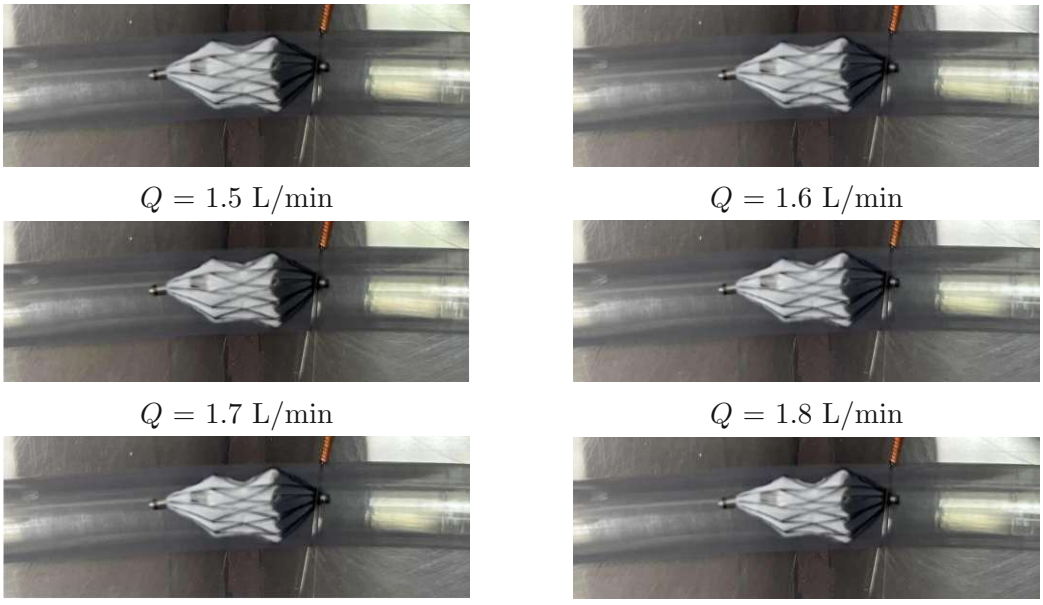

Figure 3.7: *Image series of MVP's diameter size reduction with increasing flow rate (from 0.1 to 2 L/min). The series was taken during the experiment with the MVP with two holes in the low-compliance, 6 mm diameter pipe. The two support structures to prevent migration are visible downstream of the device.*

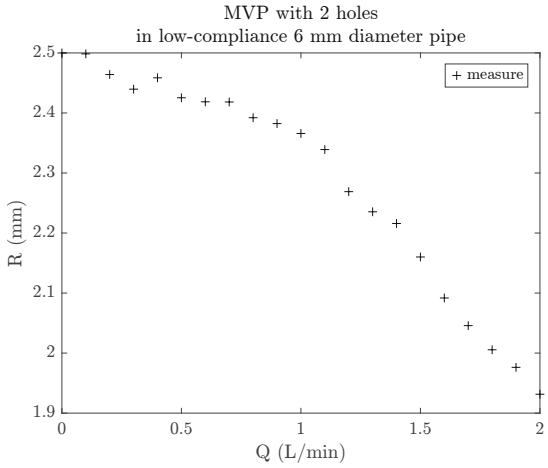

Figure 3.8: *MVP radius as a function of the volume flow rate. The proximal diameter of the MVP decreases with increasing flow rate. The measurements were performed under JMicroVision software.*

Die approbierte gedruckte Originalversion dieser Diplomarbeit ist an der TU Wien Bibliothek verfügbar
The approved original version of this thesis is available in print at TU Wien Bibliothek.

3.2 Numerical Results

The CFD simulations were run until the stabilisation of the pressure drop between the inlet and outlet was reached. For every configuration of the MVP (no, one and two orifices), ten simulations were run for different inlet flow rates from 0.1 to 1 L/min. Figure 3.9 shows the comparison of the measurements with the in vitro experiments.

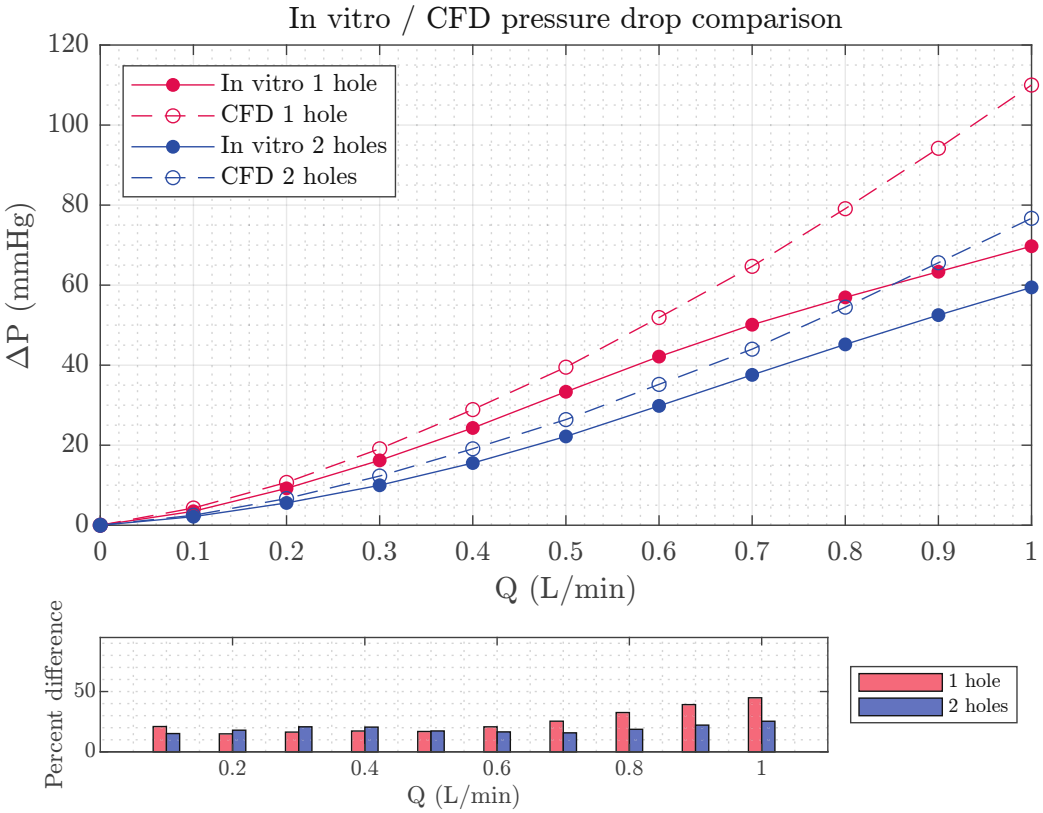

Figure 3.9: *Comparison of the pressure drop obtained in the simulations with the pressure drop obtained during the in vitro analysis in the 5 mm diameter pipe. Below, the percent difference between the two measurements for each flow rate are reported.*

A correlation can be appreciated in Figure 3.9 for the MVP with one hole (RMSE = 2.5 mmHg, for flow rates up to 0.4 L/min) as well as for the MVP with two holes (RMSE = 2.0 mmHg, for flow rates up to 0.4 L/min). For high flow rates, the difference increases and the curves deviate from one another. This divergence can be measured in terms of percent difference. The percent difference between in vitro and CFD results increases from 15% to

Die approbierte gedruckte Originalversion dieser Diplomarbeit ist an der TU Wien Bibliothek verfügbar
The approved original version of this thesis is available in print at TU Wien Bibliothek.

45% for the one hole configuration, and from 15% to 25% for the two holes configuration.

Good matching between the in silico and in vitro measurements in terms of pressure drop allowed to further look into the other simulations outcomes. The velocity fields, the low velocity zones, the wall shear stresses and the static pressure acting on the external surface of the MVP are displayed in the flowing figures. Concerning the velocity fields in Figure 3.10, similar patterns can be observed for the one and two holes configurations, hence recirculation patterns inside the MVP avoiding stagnation. Whereas for no hole configuration, a low velocity zone can be seen in the internal cavity of the MVP. Similar observations are confirmed by looking for the low velocity zones in Figure 3.11, in which regions of extreme low velocity are highlight in red ($v < 0.1$ m/s).

Die approbierte gedruckte Originalversion dieser Diplomarbeit ist an der TU Wien Bibliothek verfügbar
The approved original version of this thesis is available in print at TU Wien Bibliothek.

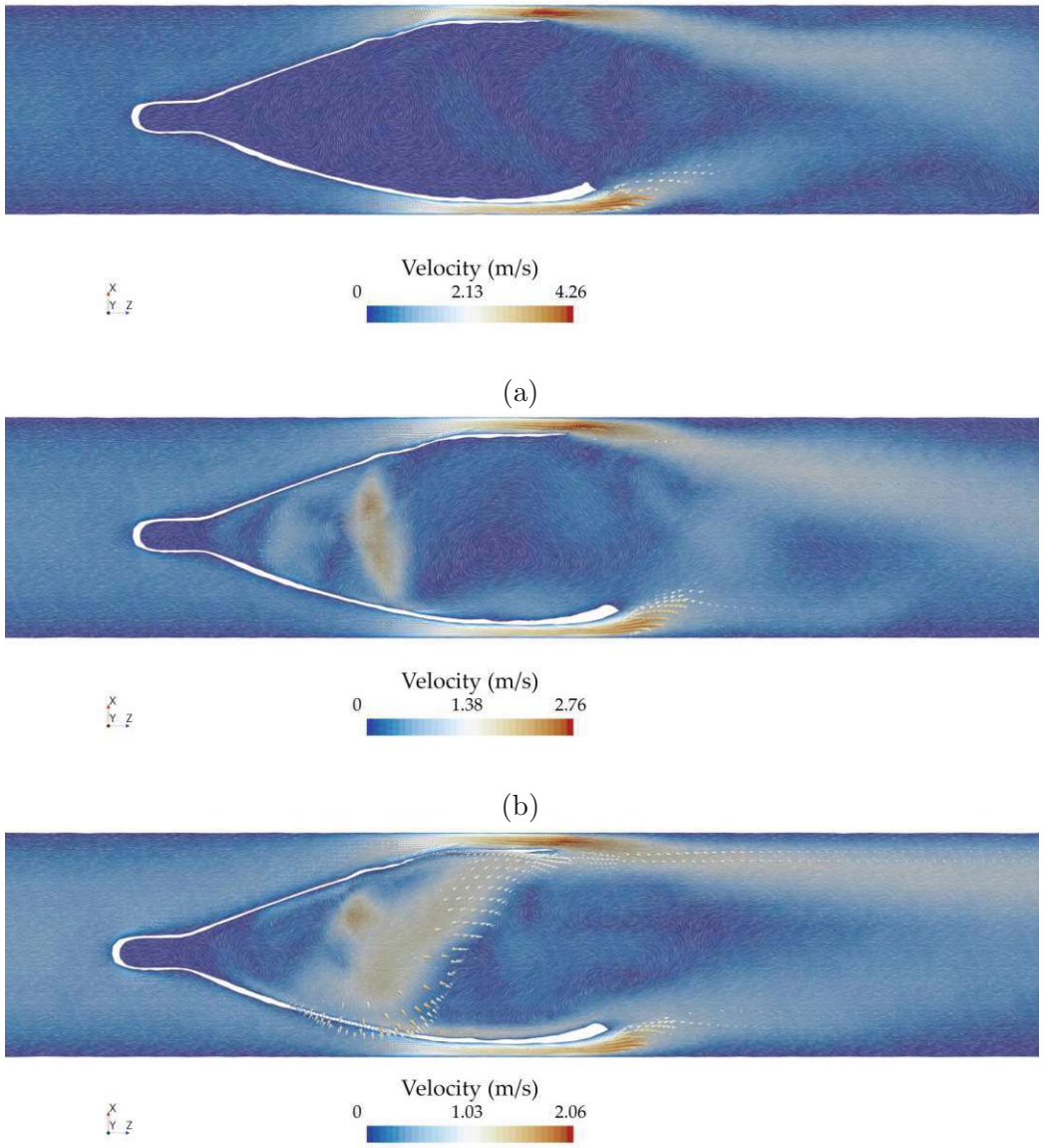

Figure 3.10: *Computational Fluid Dynamics simulated flow velocity fields for $Q = 0.5$ L/min of the MVP with (a) no hole, (b) 1 hole and (c) 2 holes. The velocity fields are displayed as line integral convolution with superimposed velocity vectors on a single cut plane along the longitudinal axis of the MVP, revealing some recirculation flow inside the MVP with 1 and 2 holes whereas prominent stagnation flow inside the MVP with no hole. The dark blue regions revel low velocities, as the brown colour stands for high velocity regions.*

Die approbierte gedruckte Originalversion dieser Diplomarbeit ist an der TU Wien Bibliothek verfügbar
The approved original version of this thesis is available in print at TU Wien Bibliothek.
TU Bibliothek Your knowledge hub WIEN

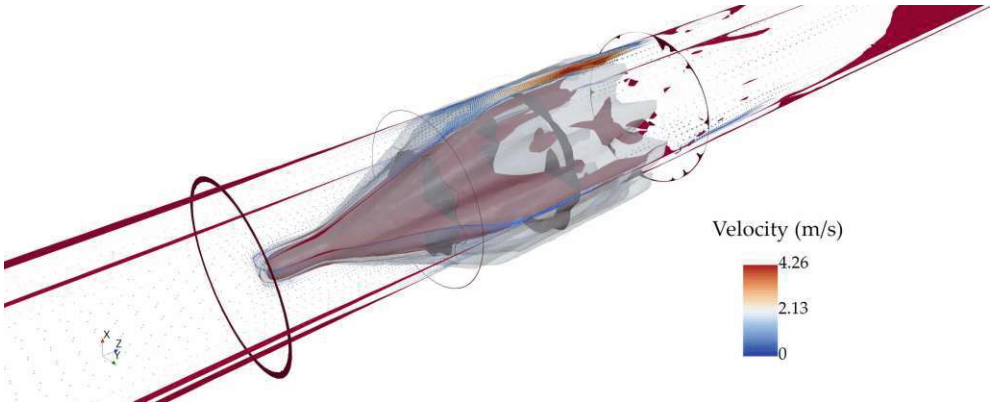

(a)

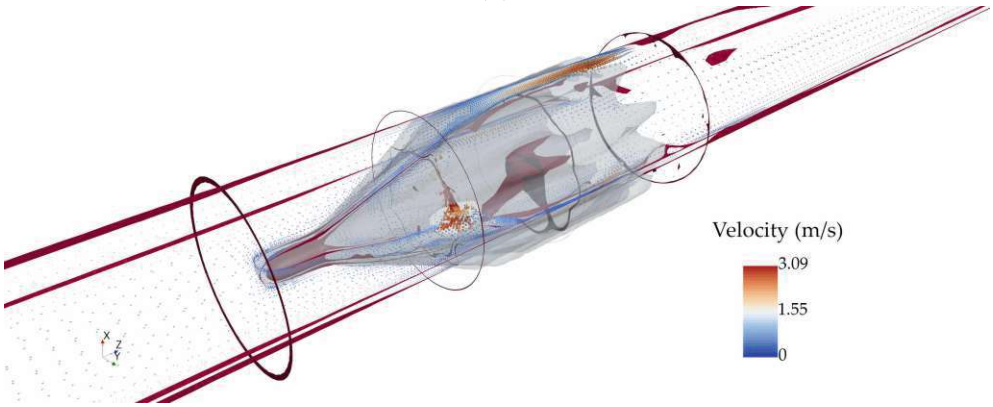

(b)

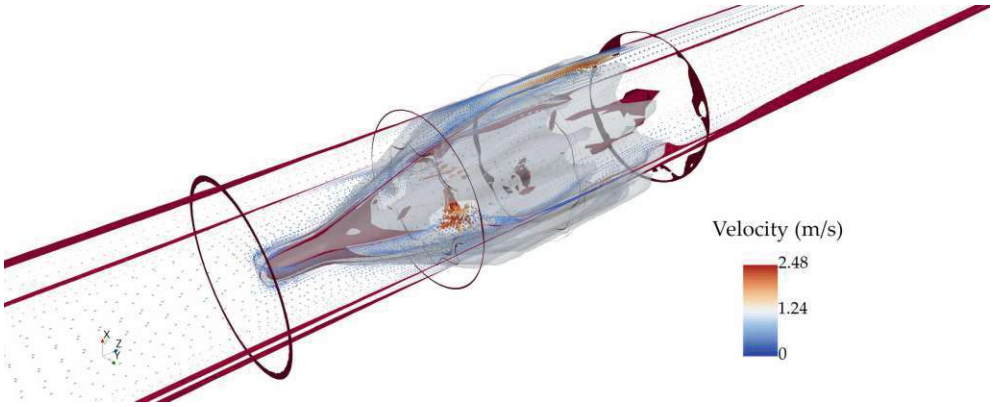

(c)

Figure 3.11: *Computational Fluid Dynamics simulated stagnation flow regions for Q = 0.5 L/min of the MVP with (a) no hole, (b) 1 hole and (c) 2 holes. The dark red colour highlights the regions where the velocity is below 0.1 m/s. Stagnation occurs massively inside the MVP with no hole. No prominent stagnation zones developed in MVP with 1 and 2 holes.*

Die approbierte gedruckte Originalversion dieser Diplomarbeit ist an der TU Wien Bibliothek verfügbar
The approved original version of this thesis is available in print at TU Wien Bibliothek.
TU Bibliothek Your knowledge hub WIEN

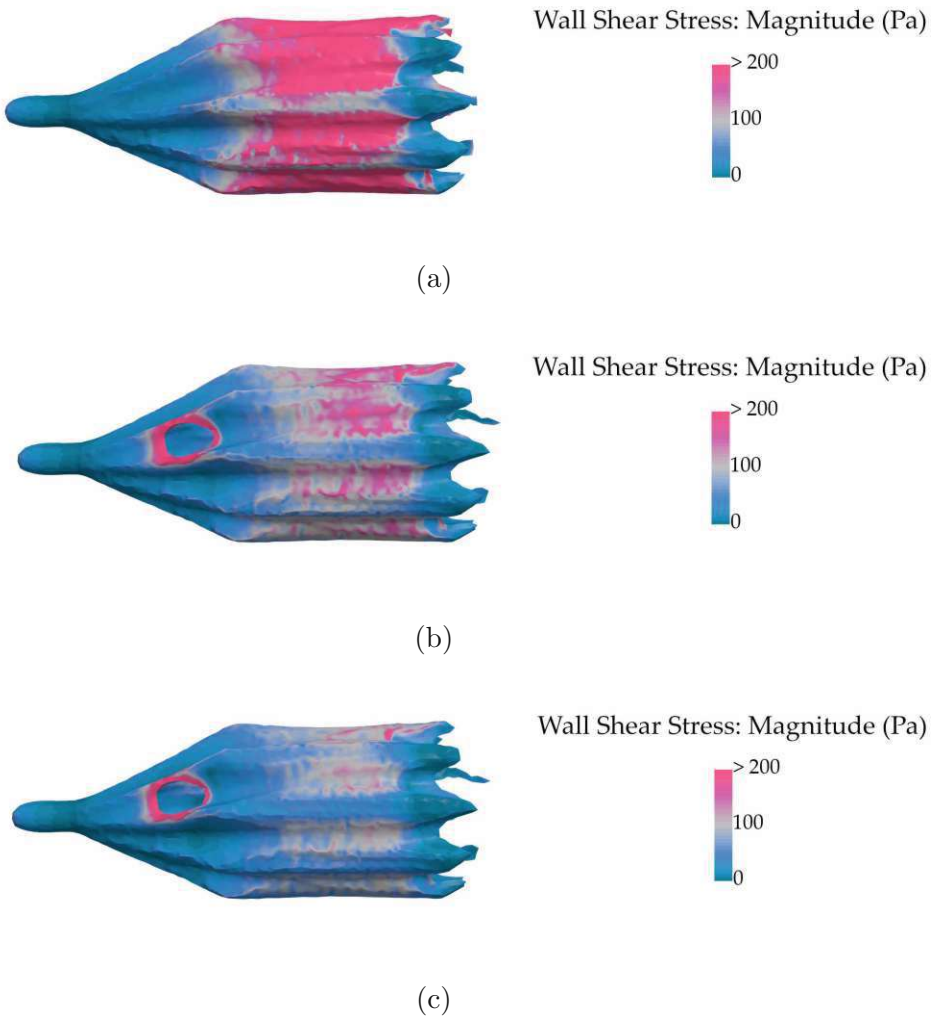

Figure 3.12: *Computational Fluid Dynamics simulated wall shear stress, for Q = 0.5 L/min, acting on the surface of the MVP with (a) no hole, (b) 1 hole and (c) 2 holes. Higher wall shear stresses occur at the medial cylindrical part of the MVP with one hole. The shear stresses diminish with increasing number of holes. For MVP with 1 and 2 holes, higher wall shear stresses occur around the hole(s).*

Die approbierte gedruckte Originalversion dieser Diplomarbeit ist an der TU Wien Bibliothek verfügbar
The approved original version of this thesis is available in print at TU Wien Bibliothek.

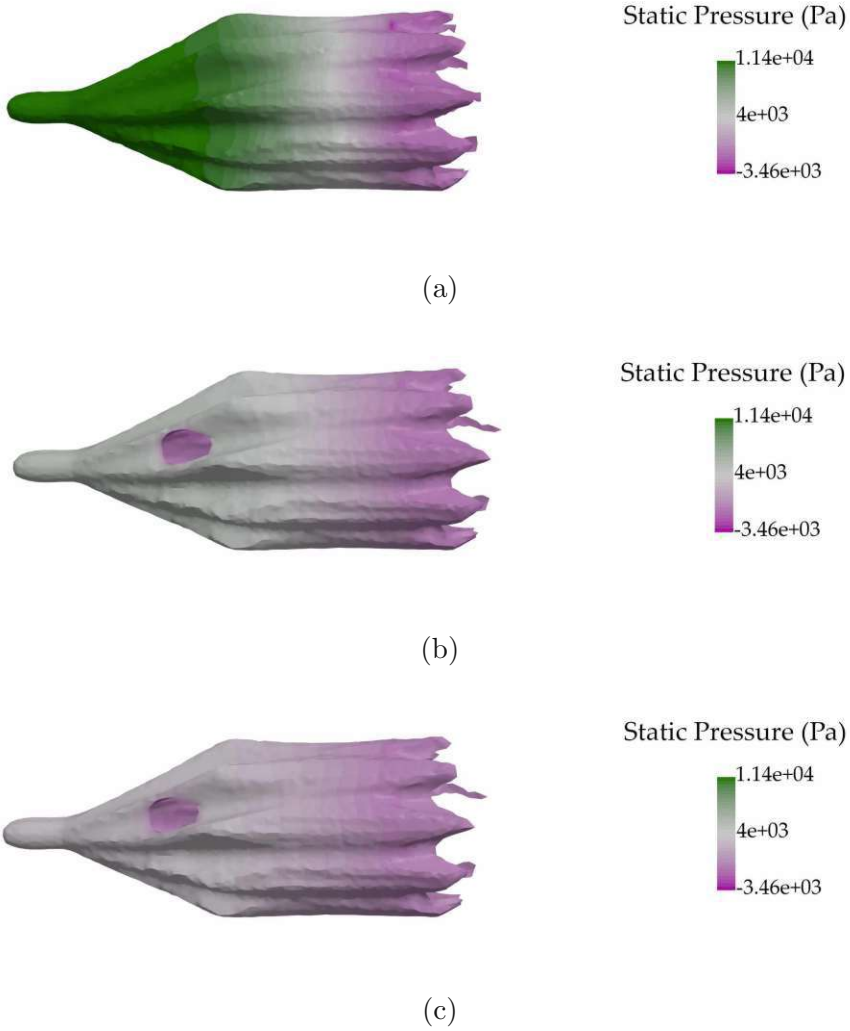

Figure 3.13: *Computational Fluid Dynamics simulated static pressure, for Q = 0.5 L/min, acting on the surface of the MVP with (a) no hole, (b) 1 hole and (c) 2 holes. Higher pressure occurs at the proximal end of MVP (*$1.15.10^4$ *Pa) then decreases with addition of holes (*$3.5.10^3$ *Pa) recording a 107% difference decrease.*

Die approbierte gedruckte Originalversion dieser Diplomarbeit ist an der TU Wien Bibliothek verfügbar
The approved original version of this thesis is available in print at TU Wien Bibliothek.

3.3 Washout Outcome

The average content of old blood over time within the pump domain is shown in Figure 3.14. For the one and two holes configurations, 95% of the old blood passive scalar was washed out in 0.48 seconds. In the no hole configuration, the residence time was only slightly longer, so that 95% of the blood was washed out in 0.6 seconds. In Appendix F, snapshot series on a single plane along the longitudinal axis for the three MVPs' configurations show how new blood replaces old blood in the fluid region.

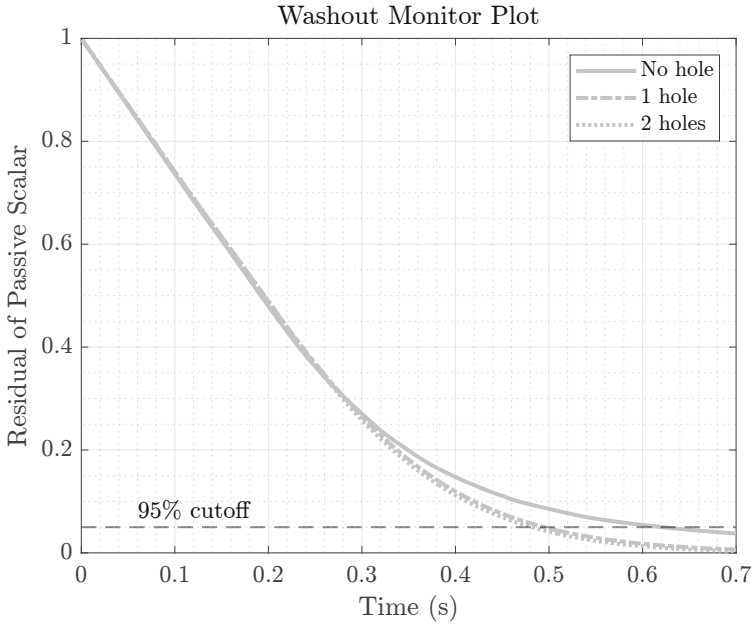

Figure 3.14: *Residence blood time. Time course of residual volume of the passive scalar simulating "old blood" being replaced by "new blood" inside the fluid region of the numerical model. At t = 0 s, all cells are marked with a 1. As "old blood" is replaced by the "new blood", cells change their value to 0. For a MVP with no hole, the blood is flushed at 95% after 0.6 seconds. It takes about 0.48 seconds in the case of the MVP with 1 or 2 holes.*

3.4 Thrombus Risk Formation

The thrombus risk formation model led to the visualisation of the AP accumulation regions in which the concentration increased above a certain threshold. For improved readability, the AP specie was scaled such that a part per million (ppm) increase in relation to the initial value of 25e12 m^{-3} was visible,

Die approbierte gedruckte Originalversion dieser Diplomarbeit ist an der TU Wien Bibliothek verfügbar
The approved original version of this thesis is available in print at TU Wien Bibliothek.

and this scaling is kept consistent throughout this work[3]. In Figure 3.16, the pipe and the MVP geometries are in grey, whereas regions of scaled AP concentration above 3.2 are shown in pink.

Only small volumes of elevated scaled AP concentration are located upstream the MVP close to its proximal end, whereas more important and larger volumes can be seen downstream the MVP. In Figure 3.15, the volume averaged scaled AP concentration for each of the three MVP configurations is displayed.

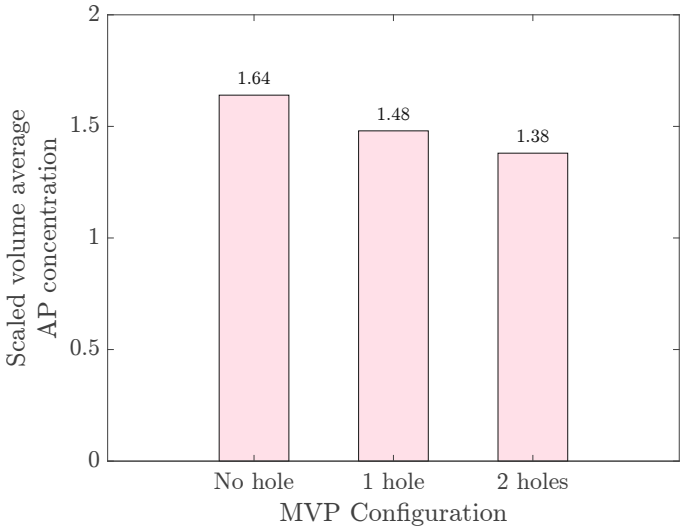

Figure 3.15: *Scaled volume average of the AP concentration for each of the three MVP configurations.*

The scaled volume average of AP concentration decreases with the number of MVP's hole(s).

[3]The scaling is simply: $\left(\frac{\phi_a - \phi_{a,\text{initial}}}{\phi_{a,\text{initial}}}\right) \times 10^6$.

Die approbierte gedruckte Originalversion dieser Diplomarbeit ist an der TU Wien Bibliothek verfügbar
The approved original version of this thesis is available in print at TU Wien Bibliothek.

(a)

(b)

(c)

Figure 3.16: *Computational Fluid Dynamics for the thrombus risk model. Scaled AP concentration in the grey pipe and MVP geometry for Q = 0.5 L/min. All the volumes above the threshold 3.2 are shown in pink for the MVP with no hole (a), 1 hole (b) and 2 holes (c).*

Die approbierte gedruckte Originalversion dieser Diplomarbeit ist an der TU Wien Bibliothek verfügbar
The approved original version of this thesis is available in print at TU Wien Bibliothek.
TU Bibliothek Your knowledge hub WIEN

Chapter 4

Discussion

The MVP used as a PFR is becoming increasingly interesting for clinicians as a bridging strategy to palliative surgery. The customisation of its PTFE membrane makes it a workable option for the reduction of pulmonary circulation to get the Q_p/Q_s ratio under control. This study aimed to hydraulic characterise three configurations of the device (no, one and two holes) to accomplish a first step towards the understanding of device personalisation throughout in vitro experiments and in silico simulations.

Flow distribution

In the wake of the work by Kizilski et al., we further conducted in vitro experiments with an array of MVP devices with three different fenestration types in different pipe sizes and compliances to form a matrix of data. We measured the pressure drop in steady state for flow rates up to 2 L/min for each of the MVP configurations in each of the pipes. Overall, the observations made were similar to the ones reported by Kizilski et al. The experiments showed a highly dependent pressure drop upon vessel diameter. The smaller the vessel diameter in which the MVP was deployed, the higher the pressure drop. In a smaller vessel, the MVP exerts a greater radial force. Since the device behaves like a spring, compressing it further increases resistance as it strives to return to its original configuration. For an MVP in an advanced compressed state - due to positioning into a smaller vessel -, the pressure drop, accounting for the force needed to further compress it, is higher.

Experiments with the unperforated MVP showed an immediate difference of pressure drop related to pipe diameter at low flow rates. At 0.2 L/min, for the 4.8 mm diameter pipe, the pressure drop is already 20 mmHg. This immediate difference arising at very low flow rates reflects the high resistance of the device. For the no hole configuration, if the only way for the fluid to

Die approbierte gedruckte Originalversion dieser Diplomarbeit ist an der TU Wien Bibliothek verfügbar
The approved original version of this thesis is available in print at TU Wien Bibliothek.

flow through the device is as paraflow, the radial force that the device can produce plays a very important role in influencing the pressure drop. The pipe diameter is in this case mostly relevant because a higher radial force is produced when the pipe diameter is smaller and the resulting pressure drop is consequently higher, as we observed for the pipe of 4.8 mm in diameter.

Another factor contributing to the pressure drop is pipe compliance. Even though we were not able to measure it quantitatively, we were able to conduct qualitative assessments. The difference between the two 6 mm diameter pipes was appreciable. The more compliant pipe featured a slightly smaller pressure drop in all three of the MVP configurations for all flow rates. One reason is that a compliant pipe can expand to accommodate for the flow without increasing the pressure drop across its length.

All the experiments for the MVP with one and two holes showed two distinct flow pattern distributions along the range of measured flow rates. At low flow rates, up to 0.4–0.5 L/min, we observed a quadratic dependency of the pressure with the flow. Then, for flows higher than 1.2 L/min, the tendency changes. From an initial convex curve, we get to a concave curve for which the pressure drop still increases but at a slower paste.

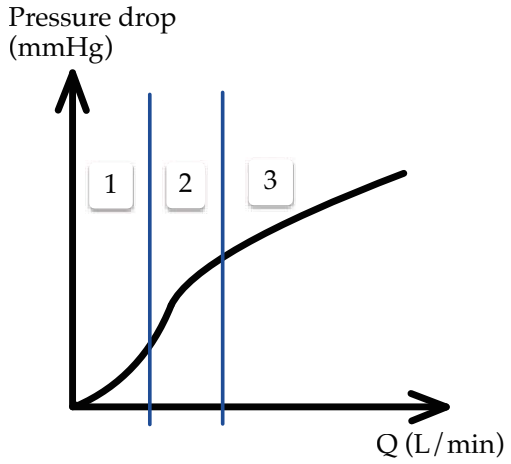

Figure 4.1: *Sketched Pressure-Flow curve distribution for a MVP with one hole. At low flow rates (1), the fluid flows mainly through the hole. At high flow rates (3), the fluid flows mainly as paraflow. In between is the transition region (2), the fluid flows both through the hole and as paraflow.*

The flow distribution is responsible for these observations. At low flow rates, fluid flows mainly through the hole(s). This assumption is supported

Die approbierte gedruckte Originalversion dieser Diplomarbeit ist an der TU Wien Bibliothek verfügbar
The approved original version of this thesis is available in print at TU Wien Bibliothek.

by the evidence of the analytical formula of the pressure-flow relationship for a flow through a hole, in which we observe a correlation of the analytical formula with the in vitro experimental results. At higher flow rates, the pressure field that develops in the fluid region gets higher than the radial force the device can exert. The device diameter starts to reduce. The effective fenestration size of the device gets smaller: flow through the hole diminishes, whereas the paraflow increases as the device diameter shrinks. At higher flow rates, we assume that the flow through the orifice is negligible compared to the paraflow. The quadratic relationship between the pressure drop and the flow rate is lost.

In Figure 4.1 we reconstruct by hand how the theoretical curve for a MVP with one hole should look like.

Measurments in the 3D-printed geometry

As we made all the previous measurements in the straight pipes, we wanted to perform the same ones in a 3D-printed geometry with the MVP placed in the RPA of the printed vasculature. The goal of having the measurements of pressure and flow rates in a 3D-printed geometry cropped from a HLHS patient was to test the hydraulic characteristics of the PFR in a more realistic environment. Even if it is less clear to see, it is possible to distinguish in this case the two flow phases as well.

Compared to the 4.8 mm pipe experiment, Overall, the pressure drop across the measured flow rates is close to the one in the 5 mm pipe (RMSE = 2.9 mmHg). Reasons for differences are the curves in the vasculature and the non-ideal flow profiles.

In Silico Analysis

The performed CFD simulations helped to further study haemodynamics, velocity and pressure fields arising in the fluid region occupied by the MVP and asses the hemocompatibility of the device. The comparison of simulated pressure drop displayed matching results with in vitro experiments up to 0.4-0.5 L/min. For higher flow rates, the results diverged. This observation is in line with the flow distribution we previously assumed. As the simulations were performed, the MVPs with no, one and two holes were not allowed to display any movement, hence no reduction of its diameter could occur. The geometries were fixed regardless of the initial condition on the flow rate at the inlet, thus regardless of the pressure drop as well. This is in contrast with the in vitro experiments, in which we saw a reduction of the device diameter as the pressure drop was increasing.

Die approbierte gedruckte Originalversion dieser Diplomarbeit ist an der TU Wien Bibliothek verfügbar
The approved original version of this thesis is available in print at TU Wien Bibliothek.
TU Bibliothek Your knowledge hub WIEN

At low flow rates, we assumed that most of the fluid would flow primarily through the hole(s), an idea confirmed by our in silico results. At these lower flow rates, the pressure field on the surface of the MVP remains smaller than the radial force exerted by the device, allowing the MVP's nitinol structure to retain its initial configuration. Constrictions begin only as the transmural pressure increases. However, since our in silico model cannot capture any movement or deformation of the MVP, at higher flow rates, the pressure drop continues to rise as if fluid was still flowing exclusively through the hole(s). Consequently, when comparing the in silico data to in vitro results, we infer that at flow rates above 0.5 L/min, the fluid begins its transition to paraflow (Figure 4.2).

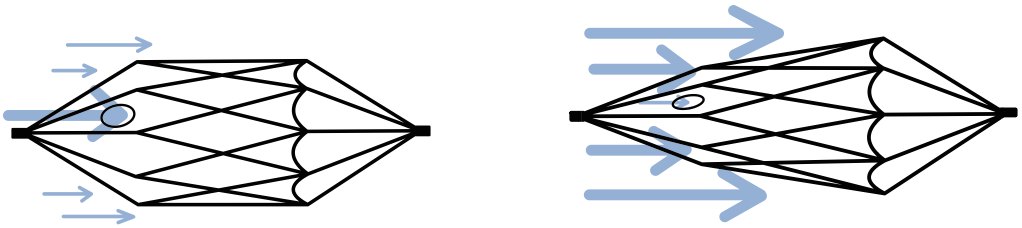

(a) (b)

Figure 4.2: *Drawings of the two flow distributions. Mostly flow through the hole in (a) versus mostly paraflow in (b). With increasing paraflow resulting from an increase in the transmural pressure between the outer and inner surface of the MVP, the diameter of its proximal end is reduced.*

The size of the holes plays an important part in the establishment of the pressure drop and consequently the hydraulic resistance of the MVP. For a different hole size, all other parameters kept constant, a higher pressure drop will arise from the MVP with the smaller hole. We tried to match as best as we could the sizes in the in silico and in vitro setup. However, the holes were smaller in the in silico experiments, a reason why the pressure drop is higher compared to the in vitro measures.

If we consider once more the results obtained by Kizilski et al., the intended size range for the circular cautery hole in their case was 1-1.5 mm, compared to ours 2 mm. This is one reason why the pressure drop is overall higher in their study (see Figure 4.3).

These findings underline how the hydraulic characteristic can be tailored to reach a targeted pressure drop. By adjusting the number of holes and the

Die approbierte gedruckte Originalversion dieser Diplomarbeit ist an der TU Wien Bibliothek verfügbar
The approved original version of this thesis is available in print at TU Wien Bibliothek.

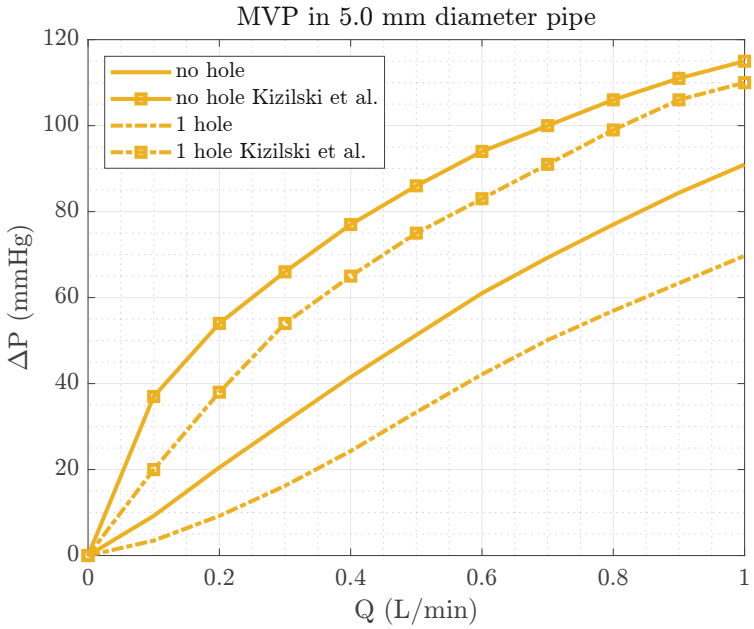

Figure 4.3: *Measurements comparison with the results by Kizilski et al. Kizilski et al. used MVPs with smaller hole diameter (1-1.5 mm) compared to ours (2 mm). This could be a reason explaining such a difference observed between the two measurments.*

hole-to-vessel diameter ratio, one can reach a wide panel of pressure drop. As device migration is also an important factor to deal with, our data provided additional information helping to tackle the issue. Migration starts when the device loses contact with the vessel walls, plummeting its friction coefficient value to 0. Therefore, as long as the fluid flows mainly through the hole, there should not be any migration risk. The risk increases with increasing paraflow, hence with increasing transmural pressure acting on the PTFE membrane. In all our experiments except the one in the 3D-printed geometry, we used support structures to prevent the device from migrating. Nonetheless, no migration was observed in the 3D-printed realistic vasculature. We suppose this to be due not because there would not be any in real case, but because the friction coefficient between the device and the 3D printing material was able to withstand the radial and axial forces that would have induced the device into distal migration.

In silico simulations were performed to study the hemodynamic behaviour of blood flow, examining patterns such as the velocity field and blood stagnation zones. The simulation results highlighted that the unperforated MVP functioned as a plug, aligning with the manufacturer's design intent. In com-

Die approbierte gedruckte Originalversion dieser Diplomarbeit ist an der TU Wien Bibliothek verfügbar
The approved original version of this thesis is available in print at TU Wien Bibliothek.

parison to configurations with one and two holes, a significant low-velocity region developed within the unperforated MVP. Without a gap between the device and the pipe walls to permit fluid flow around the unperforated device, we would observe a complete no-flow region downstream. When a single hole was introduced, fluid begin to flow through the orifice, minimizing recirculation within the device cavity. A washout analysis using a passive scalar approach confirmed our initial observations: the presence of a hole substantially improve washout, with a second hole contributing only marginally. Specifically, the passive scalar plot showed that 95% of the "old blood" was cleared after approximately 0.48 seconds for both the one- and two-hole configurations, while the no-hole case required a longer time: 0.6 seconds. The difference between these two times is only small because the washout was performed in the whole pipe. If the analysis had been limited to a smaller section of the pipe -starting just before the MVP and ending immediately after- the difference in washout times would have been more significant.

At the same overall flow, the wall shear stresses acting on the MVP surface indicate, as expected, that adding a hole enables flow through it, reducing paraflow. This effect is illustrated in Figure 3.12, where the addition of holes results in a decrease in wall shear stresses along the outer cylindrical surface of the MVP. The static pressure results similarly reveal the impact of perforation choices on the MVP surface; as more holes are introduced, the pressure on the outer surface diminishes. Notably, the distribution of pressure drop on the MVP in Figure 3.13a aligns with the size reduction of the device observed during in vitro experiments in Figure 3.7.

From the pictures taken, the reduction of the MVP's proximal diameter for the two holes configuration was measured as well. The reduction in the proximal diameter is considerably more pronounced than that in the distal diameter. In the model representing the maximum pressure gradient the device could withstand (Appendix B, Figure B.1b), Kysilsky et al. assumed a pressure distribution on the cylindrical outer surface of the MVP as $P(x) = P_g(1 - x/L)$. This assumed distribution is reasonably well captured and validated through our observations and simulations.

Thrombus risk model

The thrombus model was adapted from the work of Blum et al., which used convection-diffusion equations for three different species: AP, NP, and ADP, as well as mechanical and chemical activation of platelets. In this model, clot formation and its influence on the flow field were excluded, with the

Die approbierte gedruckte Originalversion dieser Diplomarbeit ist an der TU Wien Bibliothek verfügbar
The approved original version of this thesis is available in print at TU Wien Bibliothek.
TU Bibliothek Your knowledge hub WIEN

increase in AP concentration serving as an indicator of thrombus formation risk. We conducted three simulations, each corresponding to a different MVP configuration, at a flow rate of $Q = 0.5$ L/min.

Given the large stagnation zone observed within the cavity of the unperforated MVP, we expected an increase in AP concentration in this region. However, the accumulation occurred mainly downstream of the device. As a result, similar to Blum et al., we hypothesized that thrombi were likely transported downstream rather than forming directly where they were observed.

For the three configurations studied, the volume average AP scaled concentration decreases with number of holes. For the MVP with one and two holes, the concentration difference is minimal, only about 7%, indicating no significant difference in thrombus formation potential between these two configurations. In all cases, the AP increase is much more pronounced downstream than upstream of the MVP. This can be explained by the fact that mechanical activation predominantly occurs in the gap region between the MVP and the pipe walls, where high shear stresses at higher velocities facilitate AP transport and downstream accumulation. Unlike Blum et al., we did not have clinical data to compare with regard to thrombus formation frequency in the pipe.

The thrombus model has certain limitations. First, likewise all the in vitro experiments, the simulations were conducted under steady-state conditions, without accounting for the heart's pulsatile flow. Second, the simulations did not incorporate potential movements of the MVP, which would occur in a dynamic physiological setting. Third, while validating the thrombus formation risk model with blood testing was beyond the scope of this project, it remains an important area for future research.

Die approbierte gedruckte Originalversion dieser Diplomarbeit ist an der TU Wien Bibliothek verfügbar
The approved original version of this thesis is available in print at TU Wien Bibliothek.
TU Bibliothek Your knowledge hub WIEN

Chapter 5

Conclusion

In this study, we investigated three different MVP configurations through a combination of in vitro experiments and in silico simulations to assess their hydraulic properties. From these measurements, we generated plots as an initial step in building a data matrix, incorporating variables such as vessel diameter and vessel compliance. Our findings show that the MVP is responsible for a two stage flow distribution - low flow rate through hole(s) / high flow rate as paraflow - and indicate that the hydraulic properties of the MVP can be tailored by adjusting the number of holes and the MVP-to-vessel diameter ratio. Additionally, the simulations revealed the benefits of having perforations as wall shear stress, washout time, and thrombus formation risk were improved.

Future research should focus on integrating these considerations along with patient-specific data to further refine the approach. Ultimately, this will support the optimization of MVP configurations for individual cases, paving the way for a personalized, patient-specific approach.

Die approbierte gedruckte Originalversion dieser Diplomarbeit ist an der TU Wien Bibliothek verfügbar
The approved original version of this thesis is available in print at TU Wien Bibliothek.
TU Bibliothek Your knowledge hub WIEN

Acknowledgments

I would like to express my gratitude to Marcus Granegger for his generous availability for discussion and guidance throughout every step of this work. I am also grateful to Bernhard Semlitsch for his invaluable advice and for promptly suggesting the most appropriate revisions to improve this thesis. I extend my thanks to all my colleagues, not only for their assistance but also for their unfailing sense of humour and sympathy, which made the work all the more enjoyable.

This thesis is the result of the unwavering support of my family and friends throughout my studies. I owe a profound debt of gratitude to my parents for supporting me from Paris to Vienna, via the memorable years in Marseille. Special thanks go to Matteo, Giorgio, Nonna, and Clara for their affection and inspiration.

Niccolò Crescenti
02.12.2024, Vienna

Die approbierte gedruckte Originalversion dieser Diplomarbeit ist an der TU Wien Bibliothek verfügbar
The approved original version of this thesis is available in print at TU Wien Bibliothek.

Bibliography

[1] Jeremy Pinnell, Simon Turner, and Simon Howell. "Cardiac muscle physiology". In: *Continuing Education in Anaesthesia, Critical Care & Pain* 7.3 (2007), pp. 85–88.

[2] Anthony T Bejjani, Neil Wary, and Mingxia Gu. "Hypoplastic left heart syndrome (HLHS): molecular pathogenesis and emerging drug targets for cardiac repair and regeneration". In: *Expert opinion on therapeutic targets* 25.8 (2021), pp. 621–632.

[3] Eugenijus Kaniusas. *Biomedical Signals and Sensors I - Linking Physiological Phenomena and Biosignals*. Springer, 2012.

[4] "Cardiovascular System". In: *Encyclopedia of Toxicology (Third Edition)*. Ed. by Philip Wexler. Third Edition. Oxford: Academic Press, 2014, pp. 730–747. ISBN: 978-0-12-386455-0. DOI: https://doi.org/10.1016/B978-0-12-386454-3.00985-4. URL: https://www.sciencedirect.com/science/article/pii/B9780123864543009854.

[5] Merlin John Casper Fair. "Development of whole-heart myocardial perfusion magnetic resonance imaging". PhD thesis. Imperial College London, 2017.

[6] Dorothee Perloff et al. "Human blood pressure determination by sphygmomanometry." In: *Circulation* 88.5 (1993), pp. 2460–2470.

[7] Roland N Pittman. "Regulation of tissue oxygenation". In: (2016).

[8] World Health Organization. *The Top 10 Causes of Death*. Accessed: 2024-09-26. 2024. URL: https://www.who.int/news-room/fact-sheets/detail/the-top-10-causes-of-death.

[9] Mouhammad Yabrodi and Christopher W Mastropietro. "Hypoplastic left heart syndrome: from comfort care to long-term survival". In: *Pediatric research* 81.1 (2017), pp. 142–149.

[10] Jenifer A Glatz et al. "Impact of mitral stenosis and aortic atresia on survival in hypoplastic left heart syndrome". In: *The Annals of thoracic surgery* 85.6 (2008), pp. 2057–2062.

Die approbierte gedruckte Originalversion dieser Diplomarbeit ist an der TU Wien Bibliothek verfügbar
The approved original version of this thesis is available in print at TU Wien Bibliothek.
TU Bibliothek Your knowledge hub WIEN

[11] Hannah Bellsham-Revell. "Noninvasive imaging in interventional cardiology: hypoplastic left heart syndrome". In: *Frontiers in Cardiovascular Medicine* 8 (2021), p. 637838.

[12] David R Jobes et al. "Carbon dioxide prevents pulmonary overcirculation in hypoplastic left heart syndrome". In: *The Annals of thoracic surgery* 54.1 (1992), pp. 150–151.

[13] Sarah Tabbutt et al. "Impact of inspired gas mixtures on preoperative infants with hypoplastic left heart syndrome during controlled ventilation". In: *Circulation* 104.suppl_1 (2001), pp. I–159.

[14] Alex Yartsev. *Fick's Principle of cardiac output measurement*. Accessed: 08-10-2024. 2015. URL: https://derangedphysiology.com/main/cicm-primary-exam/required-reading/cardiovascular-system/Chapter%20811/ficks-principle-cardiac-output-measurement#:~:text=The%20principle%20can%20be%20summarised,gradient)%20of%20the%20substance.%22.

[15] M Navaratnam and C Ramamoorthy. "HYPOPLASTIC LEFT HEART SYNDROME". In: *Pediatric Anesthesia: A Problem-Based Learning Approach* (2018), p. 75.

[16] Nathalie Mini, Peter A Zartner, and Martin BE Schneider. "New insights learned from the pulmonary to systemic blood flow ratio to predict the outcome in patients with hypoplastic left heart syndrome in the pre-Glenn stage: A single-center study". In: *Frontiers in Cardiovascular Medicine* 10 (2023), p. 1207869.

[17] R Elling, B Stiller, and J Grohmann. "Transcatheter device occlusion of the left ventricular outflow tract as treatment for severe aortic regurgitation in hypoplastic left heart syndrome". In: *Catheterization and Cardiovascular Interventions* 86.3 (2015), pp. 463–466.

[18] Marcus Granegger et al. "A long-term mechanical cavopulmonary support device for patients with Fontan circulation". In: *Medical engineering & physics* 70 (2019), pp. 9–18.

[19] KidsHealth Medical Experts. *The Norwood Procedure*. Accessed: 2024-02-15. 2021. URL: https://kidshealth.org/en/parents/norwood.html.

[20] KidsHealth Medical Experts. *The Glenn Procedure*. Accessed: 2024-02-15. 2021. URL: https://kidshealth.org/en/parents/glenn.html.

[21] KidsHealth Medical Experts. *The Fontan Procedure*. Accessed: 2024-02-15. 2021. URL: https://kidshealth.org/en/parents/fontan.html.

Die approbierte gedruckte Originalversion dieser Diplomarbeit ist an der TU Wien Bibliothek verfügbar
The approved original version of this thesis is available in print at TU Wien Bibliothek.
TU Bibliothek Your knowledge hub WIEN

[22] Francesca Sperotto et al. "Transcatheter palliation with pulmonary artery flow restrictors in neonates with congenital heart disease: feasibility, outcomes, and comparison with a historical hybrid Stage 1 cohort". In: *Circulation: Cardiovascular Interventions* 16.12 (2023), e013383.

[23] Rajesh Sharma. "Pulmonary artery banding: Rationale and possible indications in the current era". In: *Annals of pediatric cardiology* 5.1 (2012), p. 40.

[24] Abdul H Khan et al. "Utility of the Medtronic microvascular plug™ as a transcatheter implantable and explantable pulmonary artery flow restrictor in a swine model". In: *Catheterization and Cardiovascular Interventions* 93.7 (2019), pp. 1320–1328.

[25] Raymond N Haddad et al. "Outcomes of manually modified microvascular plugs to pulmonary flow restrictors in various congenital heart lesions". In: *Frontiers in Cardiovascular Medicine* 10 (2023), p. 1150579.

[26] Shannen B Kizilski et al. "Transcatheter Pulmonary Artery Banding in High-Risk Neonates: In-Vitro Study Provoked by Initial Clinical Experience". In: *Cardiovascular Engineering and Technology* 14.5 (2023), pp. 640–654.

[27] Chelsea Miller et al. "Modified microvascular plug as a flow restrictor in a single ventricle patient with MAPCAs". In: *Progress in Pediatric Cardiology* 72 (2024), p. 101712.

[28] Stephen Nageotte et al. "Total transcatheter stage 1: a word of caution". In: *Pediatric Cardiology* 42.6 (2021), pp. 1410–1415.

[29] Dietmar Schranz et al. "Hypoplastic left heart stage I: no Norwood, no hybrid". In: *Circulation* 142.14 (2020), pp. 1402–1404.

[30] Stefan Boës et al. "Control of the fluid viscosity in a mock circulation". In: *Artificial organs* 42.1 (2018), pp. 68–77.

[31] LF Hoyt. "New table of the refractive index of pure glycerol at 20 C". In: *Industrial & Engineering Chemistry* 26.3 (1934), pp. 329–332.

[32] John Bartlett Segur and Helen E Oberstar. "Viscosity of glycerol and its aqueous solutions". In: *Industrial & Engineering Chemistry* 43.9 (1951), pp. 2117–2120.

[33] Cadence CFD Solutions. *Y+ Boundary Layer Thickness*. Accessed: 21-10-2024. 2023. URL: `https://resources.system-analysis.cadence.com/blog/msa2023-y-boundary-layer-thickness`.

Die approbierte gedruckte Originalversion dieser Diplomarbeit ist an der TU Wien Bibliothek verfügbar
The approved original version of this thesis is available in print at TU Wien Bibliothek.
TU Bibliothek Your knowledge hub WIEN

[34] Christopher Blum et al. "An accelerated thrombosis model for computational fluid dynamics simulations in rotary blood pumps". In: *Cardiovascular Engineering and Technology* 13.4 (2022), pp. 638–649.

[35] João S Soares, Jawaad Sheriff, and Danny Bluestein. "A novel mathematical model of activation and sensitization of platelets subjected to dynamic stress histories". In: *Biomechanics and modeling in mechanobiology* 12 (2013), pp. 1127–1141.

[36] Joshua O Taylor et al. "Development of a computational model for macroscopic predictions of device-induced thrombosis". In: *Biomechanics and modeling in mechanobiology* 15 (2016), pp. 1713–1731.

[37] FC Johansen. "Flow through pipe orifices at low Reynolds numbers". In: *Proceedings of the royal society of London. series A, containing Papers of a Mathematical and Physical character* 126.801 (1930), pp. 231–245.

[38] Xavier Roothaer. "Multi-scale study of the mechanical behaviour of bearing and bone-bearing bones: towards personalization of FE human models". PhD thesis. Université Polytechnique Hauts-de-France, 2019.

Die approbierte gedruckte Originalversion dieser Diplomarbeit ist an der TU Wien Bibliothek verfügbar
The approved original version of this thesis is available in print at TU Wien Bibliothek.

Appendix A

Anatomical Planes & Directions

Terms such as "proximal" and "distal" are used to refer to the part of the MVP respectively closer and distant to the heart.

A - Sagittal plane
B - Coronal plane
C - Transverse plane
D - Longitudinal axes
1 - Proximal
2 - Distal
3 - Medial
4 - Lateral
5 - Anterior
6 - Posterior

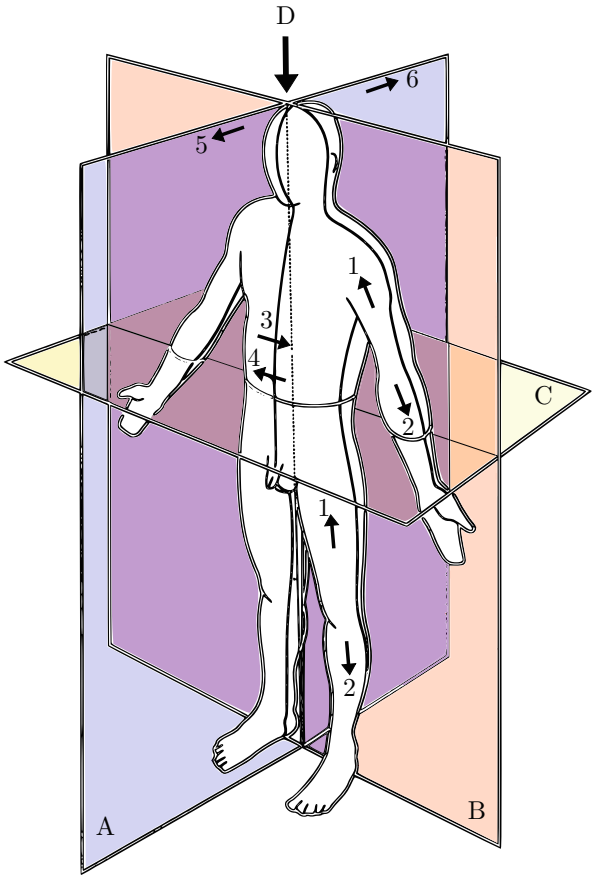

Figure A.1: *Human body, featuring anatomical planes and directions* [38].

Die approbierte gedruckte Originalversion dieser Diplomarbeit ist an der TU Wien Bibliothek verfügbar
The approved original version of this thesis is available in print at TU Wien Bibliothek.

Appendix B

Maximum Pressure Gradient

In this Appendix, we report the main steps presented by Kizilski et al. in [26] that led to the formulation of a maximum pressure gradient that the MVP can withstand before migrating.

Free Body Diagram

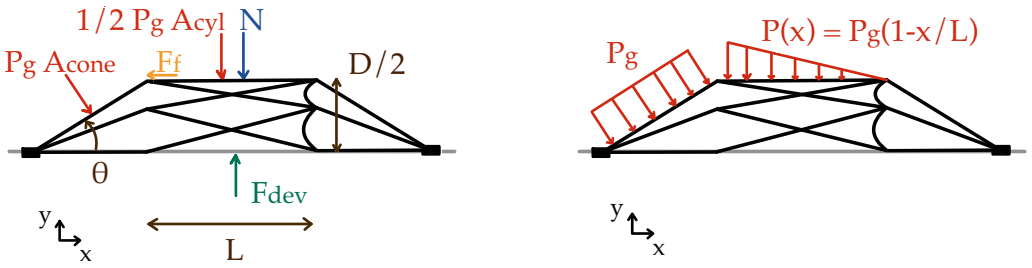

(a) Free body diagram

(b) Pressure distribution

Figure B.1: *(a) Drawing of the free body diagram of the MVP cut along its midline longitudinal axis. A Cartesian coordinate system is defined by the x-y axes. The geometrical parameters are reported in brown. The red arrows stand for the effective force derived from pressure loads, the blue arrow stands for the compressive normal force exerted by the vessel wall, the yellow arrow stands for the friction force from the vessel wall and the green arrow stands for the internal radial force F_{dev} that the device exerts to counteract compression forces. (b) Detailed representation of the pressure distribution along the MVP on its conical and cylindrical parts covered in PTFE.*

The equations of the force balance under static equilibrium refer to the

Die approbierte gedruckte Originalversion dieser Diplomarbeit ist an der TU Wien Bibliothek verfügbar
The approved original version of this thesis is available in print at TU Wien Bibliothek.

body force diagram in Figure B.1a.

Force Balance

Along the x-axis:

$$\sum F_x = 0$$

$$P_g A^x_{cone} - F_f = 0$$

$$P_g \pi (D/2)^2 - \mu N = 0 \tag{B.1}$$

Along the y-axis:

$$\sum F_y = 0$$

$$F_{dev} - P_g A^y_{cone} - \left(\frac{1}{L} \int_0^L P(x) dx \right) A_{cyl} - N = 0$$

$$F_{dev} - P_g \frac{D^2}{4 \tan(\theta)} - \frac{P_g}{2} DL - N = 0 \tag{B.2}$$

In Equation B.2, the terms can be rearranged to solve for the normal force N:

$$N = F_{dev} - P_g \frac{D}{2} \left(\frac{D}{2 \tan(\theta)} + L \right). \tag{B.3}$$

Substituting Equation B.3 for N in Equation B.1, we get the following equation, reflecting the static equilibrium of the MVP under a pressure gradient P_g:

$$P_g \pi (D/2)^2 = \mu \left[F_{dev} - P_g \frac{D}{2} \left(\frac{D}{2 \tan(\theta)} + L \right) \right]. \tag{B.4}$$

Die approbierte gedruckte Originalversion dieser Diplomarbeit ist an der TU Wien Bibliothek verfügbar
The approved original version of this thesis is available in print at TU Wien Bibliothek.

If we rearrange the terms in Equation B.4, we get the equation we were looking for, namely the maximum pressure gradient P_g^{max} the device can withstand as a function of its diameter D and its radial force F_{dev}:

$$P_g^{max} = \frac{F_{dev}}{\frac{\pi D^2}{4}\left(\frac{1}{\mu} + \frac{1}{\pi \tan(\theta)} + \frac{2L}{\pi D}\right)}. \tag{B.5}$$

To note, the length L, diameter D and angle θ are all interdependent.

Die approbierte gedruckte Originalversion dieser Diplomarbeit ist an der TU Wien Bibliothek verfügbar
The approved original version of this thesis is available in print at TU Wien Bibliothek.

Appendix C

Feedback Loop on Simulink

To perform the in vitro measurements and asses the hydraulic resistance of the MVP under different configurations, the measurements were recorded with the dSpace box coupled with the Simulink file provided in the following figures.

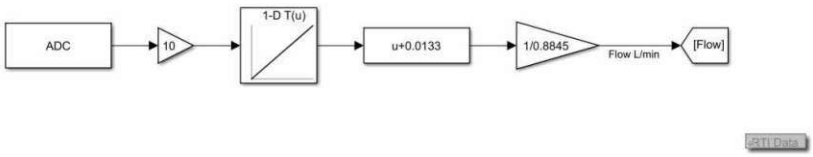

Figure C.1: *Calibration of the flow sensor.*

Die approbierte gedruckte Originalversion dieser Diplomarbeit ist an der TU Wien Bibliothek verfügbar
The approved original version of this thesis is available in print at TU Wien Bibliothek.

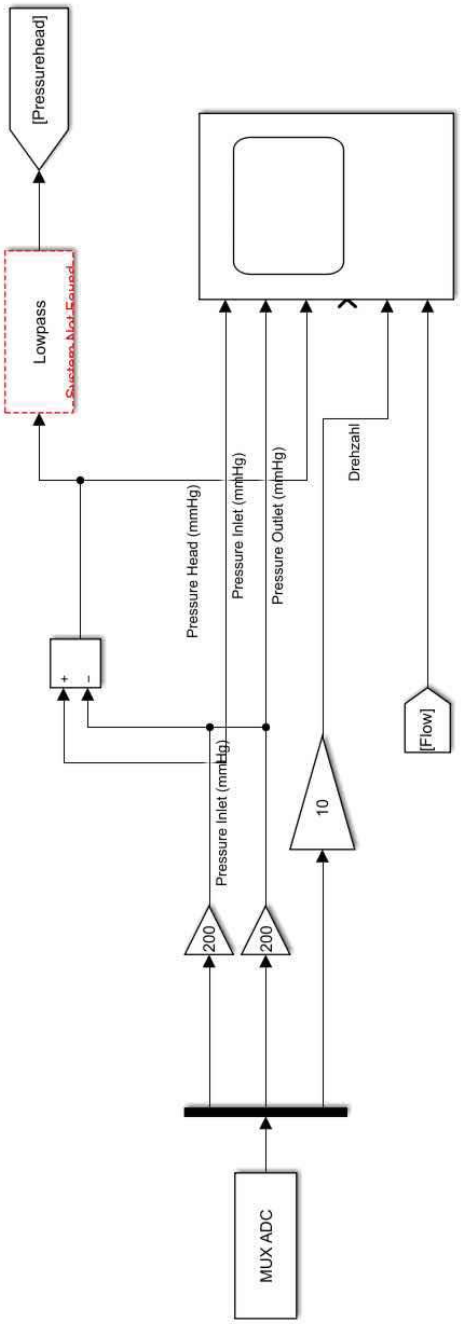

Figure C.2: *Collection of the four variables of interest on the monitor: inlet pressure, outlet pressure, pressure difference (difference between inlet and outlet pressure), and flow.*

Die approbierte gedruckte Originalversion dieser Diplomarbeit ist an der TU Wien Bibliothek verfügbar
The approved original version of this thesis is available in print at TU Wien Bibliothek.

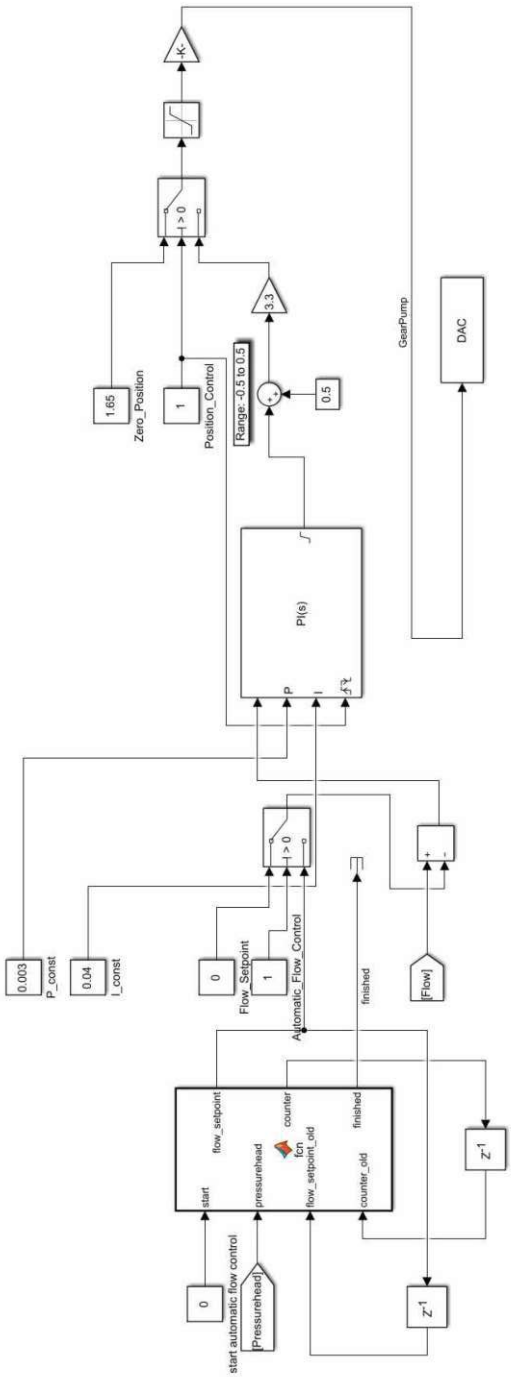

Figure C.3: *Feedback loop on the flow to control the gear pump.*

Die approbierte gedruckte Originalversion dieser Diplomarbeit ist an der TU Wien Bibliothek verfügbar
The approved original version of this thesis is available in print at TU Wien Bibliothek.
TU Bibliothek Your knowledge hub WIEN

Appendix D

Thrombus Formation Risk Model on Star CCM+

These are the codes that were implemented in the CFD software Star CCM+ for the thrombus formation risk model (under → *Tools* → *Field Functions*).

D.1 Source terms

```
% AP
AP_source = ( $ChemicalActivation * $NP + $MechanicalActivation * ( $AP + $NP ) )
% NP
NP_source = -1 * ( $ChemicalActivation * $NP + $MechanicalActivation * ( $AP + $NP ) )
% ADP
ADP_source = $R_ADP * ( $ChemicalActivation * $NP + $MechanicalActivation * ( $AP + $NP ) )
```

D.2 Mechanical and Chemical Activation

```
% Mechanical activation:
MechanicalActivation = (1 - $Phi_f) * pow($C , 1/$beta) * $beta * pow($Phi_f , ($beta - 1)/$beta) * pow($Tau , $alpha/$beta )
% Chemical activation:
```


Die approbierte gedruckte Originalversion dieser Diplomarbeit ist an der TU Wien Bibliothek verfügbar
The approved original version of this thesis is available in print at TU Wien Bibliothek.
TU Bibliothek Your knowledge hub WIEN

```
ChemicalActivation = ($ADP < $ADP_t) ? 0 : $ADP / ($ADP_t * $t_ADP)
```

D.3 Scalar Shear Stress

```
Tau = pow(3, -0.5)*

pow(

pow(${DynamicViscosity}*2*grad($$Velocity[0])[0],2)+
pow(${DynamicViscosity}*2*grad($$Velocity[1])[1],2)+
pow(${DynamicViscosity}*2*grad($$Velocity[2])[2],2)

-

(${DynamicViscosity}*2*grad($$Velocity[0])[0])*(${DynamicViscosity}*2*grad($$Velocity[1])[1]) -
(${DynamicViscosity}*2*grad($$Velocity[0])[0])*(${DynamicViscosity}*2*grad($$Velocity[2])[2]) -
(${DynamicViscosity}*2*grad($$Velocity[1])[1])*(${DynamicViscosity}*2*grad($$Velocity[2])[2])

+

3 * (
pow(${DynamicViscosity}*(grad($$Velocity[1])[0]+grad($$Velocity[0])[1]),2)+
pow(${DynamicViscosity}*(grad($$Velocity[2])[0]+grad($$Velocity[0])[2]),2)+
pow(${DynamicViscosity}*(grad($$Velocity[2])[1]+grad($$Velocity[1])[2]),2)
)

,0.5)
```


Die approbierte gedruckte Originalversion dieser Diplomarbeit ist an der TU Wien Bibliothek verfügbar
The approved original version of this thesis is available in print at TU Wien Bibliothek.

Appendix E

Error Measurements

Root Mean Square Error (RMSE)

Often mentioned in chapter 3, the RMSE between sets of values x_i and y_i is computed according to the following equation:

$$\text{RMSE} = \sqrt{\frac{1}{n}\sum_{i=1}^{n}(x_i - y_i)^2}, \tag{E.1}$$

with n the total number of data points.

Percentage Difference

Another error measurement used in this work is the percentage difference. The percentage difference between two values x and y is derived using the following equation:

$$\% = \frac{|x - y|}{\frac{x+y}{2}} \times 100. \tag{E.2}$$

Die approbierte gedruckte Originalversion dieser Diplomarbeit ist an der TU Wien Bibliothek verfügbar
The approved original version of this thesis is available in print at TU Wien Bibliothek.

Appendix F

Washout Results

The washouts of the passive scalar under Star CCM+ software for the three configurations of the MVP were conducted for an inflow rate of $Q = 0.4$ L/min.

F.1 No hole

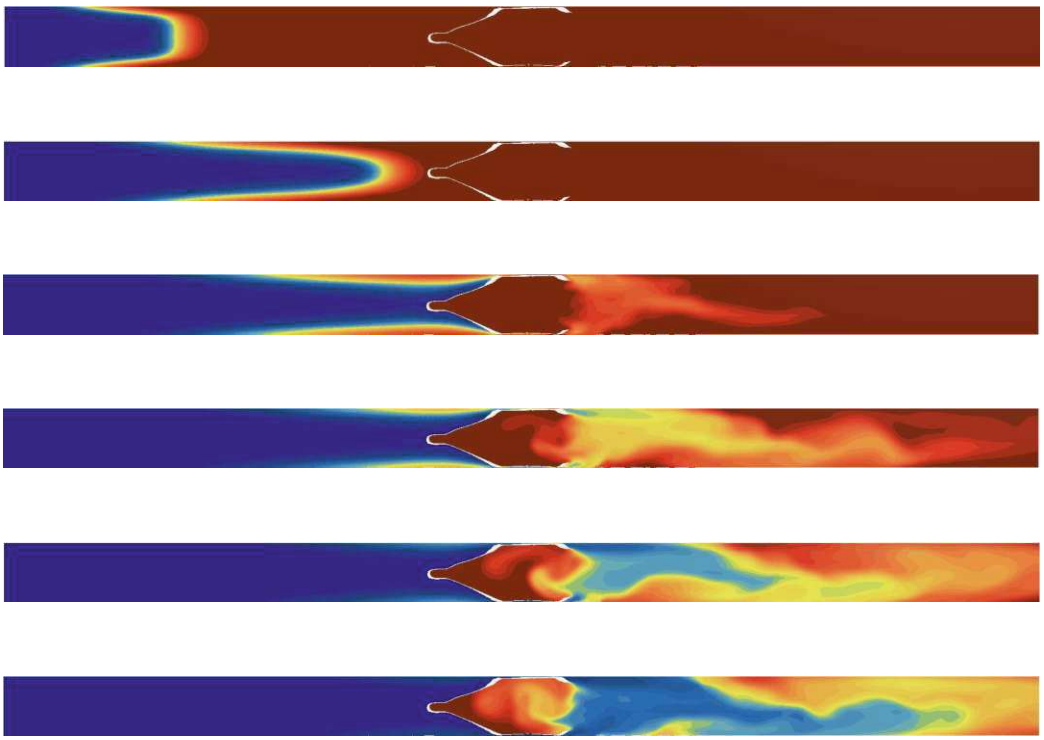

Die approbierte gedruckte Originalversion dieser Diplomarbeit ist an der TU Wien Bibliothek verfügbar
The approved original version of this thesis is available in print at TU Wien Bibliothek.

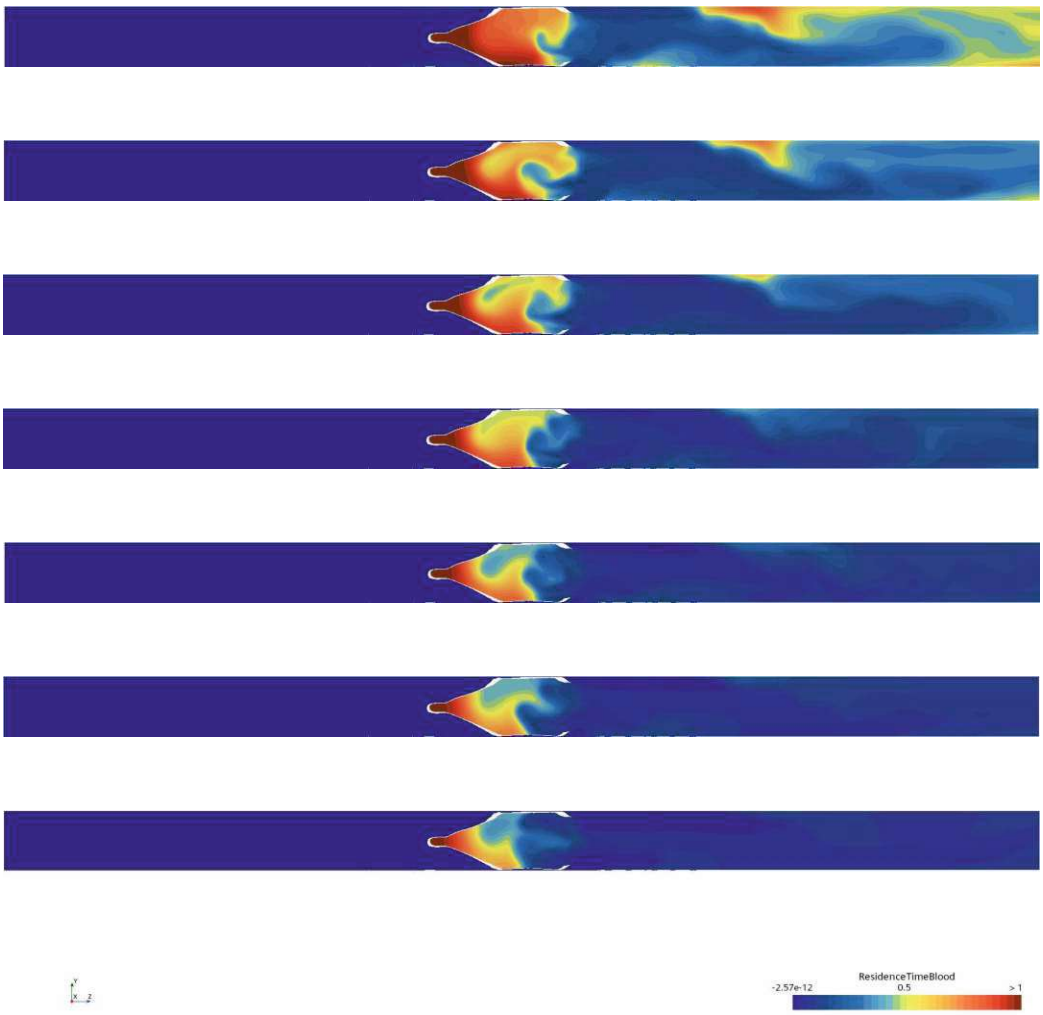

Figure F.1: *Snapshot series on a single cut plane along the longitudinal axis of the unperforated MVP in longitudinal (y-z) plane. The first snapshot being taken at 50 ms, snapshots are taken every 50 ms.*

Die approbierte gedruckte Originalversion dieser Diplomarbeit ist an der TU Wien Bibliothek verfügbar
The approved original version of this thesis is available in print at TU Wien Bibliothek.

F.2 1 hole

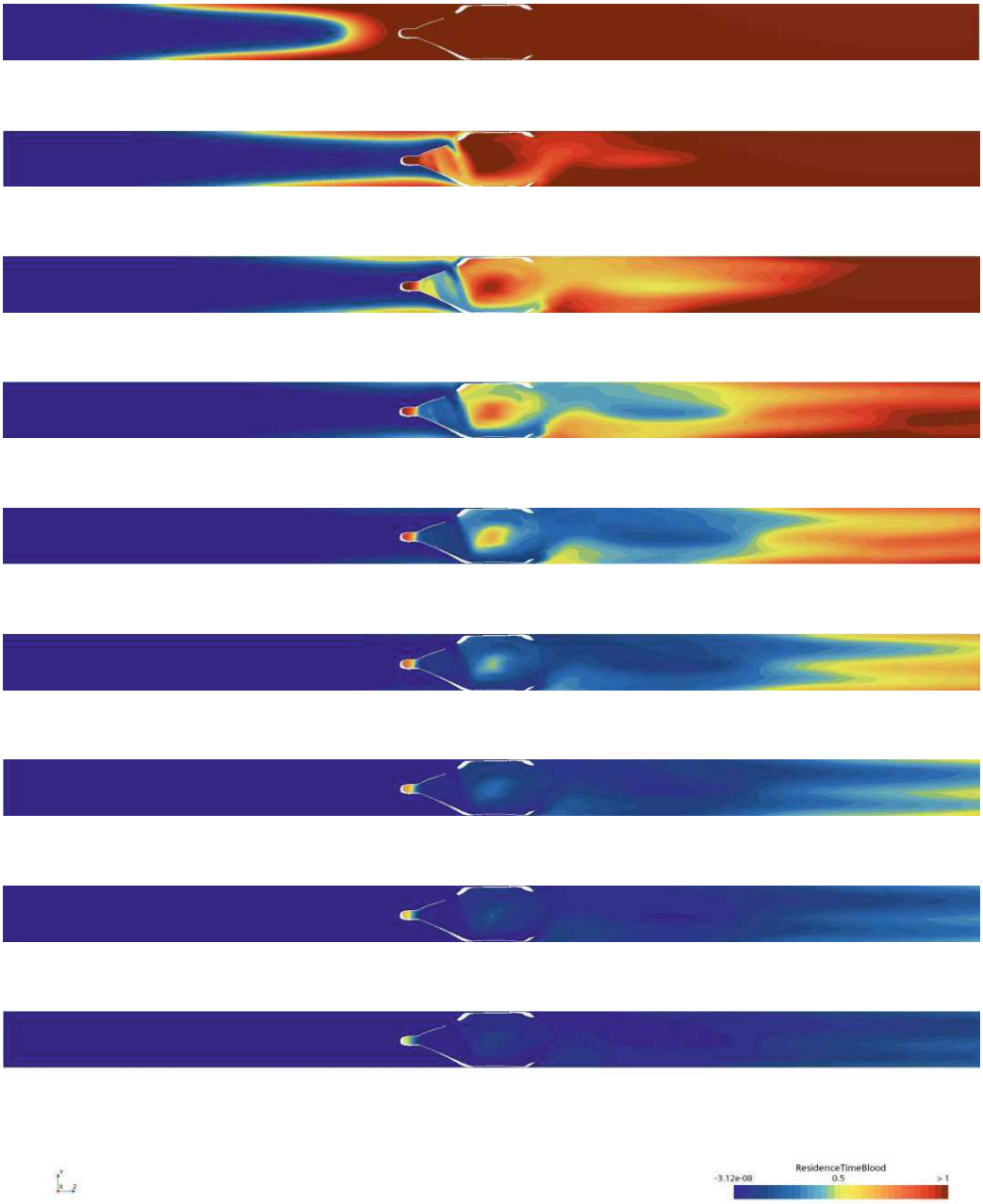

Figure F.2: *Snapshot series on a single cut plane along the longitudinal axis of the MVP with one hole in longitudinal (y-z) plane. The first snapshot being taken at 100 ms, snapshots are taken every 50 ms.*

Die approbierte gedruckte Originalversion dieser Diplomarbeit ist an der TU Wien Bibliothek verfügbar
The approved original version of this thesis is available in print at TU Wien Bibliothek.
TU Bibliothek Your knowledge hub WIEN

F.3 2 holes

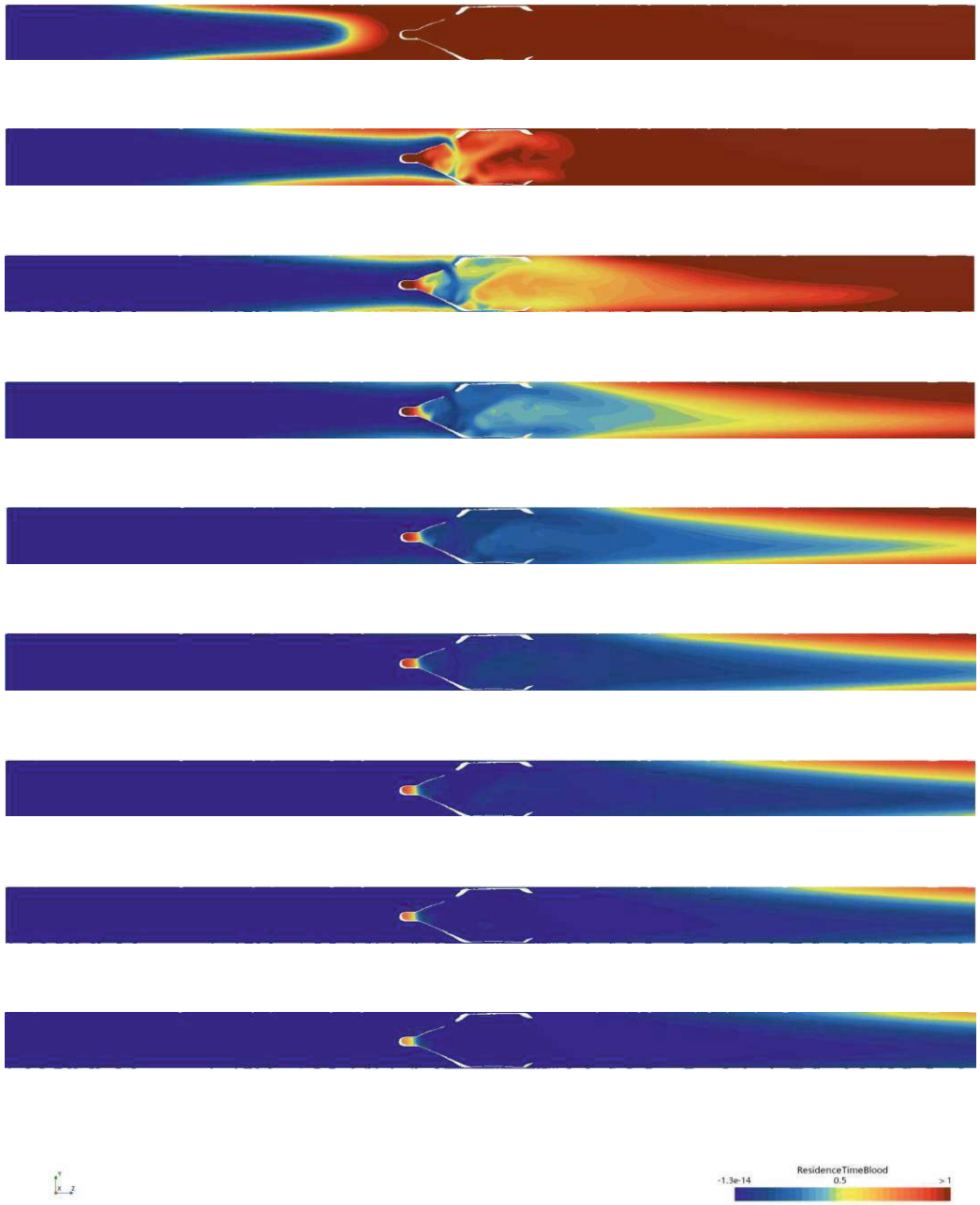

Figure F.3: *Snapshot series on a single cut plane along the longitudinal axis of the MVP with one hole in longitudinal (y-z) plane. The first snapshot being taken at 100 ms, snapshots are taken every 50 ms.*

Die approbierte gedruckte Originalversion dieser Diplomarbeit ist an der TU Wien Bibliothek verfügbar
The approved original version of this thesis is available in print at TU Wien Bibliothek.
TU Bibliothek Your knowledge hub WIEN